

Learning Polymer Crystallization with the Aid of Linear, Branched and Cyclic Model Compounds

Goran Ungar^{*,†,‡} and Xiang-bing Zeng[†]

Department of Engineering Materials, University of Sheffield, Sheffield S1 3JD, U.K., and Venture Business Laboratory, University of Hiroshima, Higashi-Hiroshima, Japan

Received July 30, 2001

Contents

I. Introduction	4157
II. Lamellar Structure and Chain Conformation	4158
A. Early Studies	4158
B. Integer Folded (IF) Forms	4159
C. Noninteger Folded (NIF) Form	4160
D. Fold- and End-Surface	4163
E. Chain Tilt	4166
F. Cyclic Oligomers	4168
G. Oligomers with Specific Endgroups	4169
H. Monodisperse Block Copolymers	4170
I. Branched Oligomers	4171
J. Binary Mixtures	4173
III. Crystallization Process and Morphology	4175
A. Stepwise Growth Rate vs Temperature Gradient	4175
B. Crystallization Rate Minima and Negative Order Kinetics	4175
C. Crystallization and Morphology	4178
D. Lamellar Thickening	4181
E. Implications for Polymer Crystallization Theory	4182
IV. Conclusions	4185
V. List of Symbols and Abbreviations	4186
VI. Acknowledgments	4186
VII. References	4186

1. Introduction

It is now universally accepted that polymers with reasonably flexible chains crystallize as thin lamellae with chain folding (see schematic drawing in Figure 1). A crystalline lamella is the basic morphological unit which, in the case of melt-crystallized polymers, is the building block of larger structures such as spherulites, row-structures, transcrystalline layers, etc. The reason that polymer crystals are thin is entirely kinetic; a thin crystal grows faster than a thick one, as the addition of short straight stretches of flexible chains presents a lower entropic barrier than the addition of long extended chains. Folding is a necessary accompaniment to lamellar morphol-

* To whom correspondence should be addressed. Phone: (44) 114 222 5457. Fax: (44) 114 222 5943. E-mails: g.ungar@sheffield.ac.uk.

† Department of Engineering Materials.

‡ Venture Business Laboratory.



Goran Ungar obtained his first degree and masters degree from the University of Zagreb, Croatia. In 1979, he obtained his Ph.D. from University of Bristol, England. His thesis was on radiation effects in polymers, under the supervision of Professor Keller. After spending several years at Ruđer Bošković Institute in Zagreb and at University of Bristol, he moved in 1989 to University of Sheffield where he now holds the post of Reader in the Department of Engineering Materials. His research interests are crystalline polymers, structure, and physical properties of liquid crystal polymers, liquid crystals, and supramolecular assemblies.



Xiangbing Zeng was born in 1971, P. R. China. He graduated in 1992 from the University of Science and Technology of China. He received his M. S. degree in condensed matter physics in 1995 at the Institute of Physics, Chinese Academy of Sciences. He received his Ph.D. degree in 2001 at the University of Sheffield. He studied lamellar structures in pure and mixed long chain *n*-alkanes and derivatives under the supervision of Dr. G. Ungar. He is working as a Research Assistant in the Department of Engineering Materials, University of Sheffield. His main research interests are polymer crystal structure, scattering methods, polymer crystallization and polymer physics.

ogy. Thus, it is kinetics driven, unlike the folding in proteins, which is thought to be thermodynamically

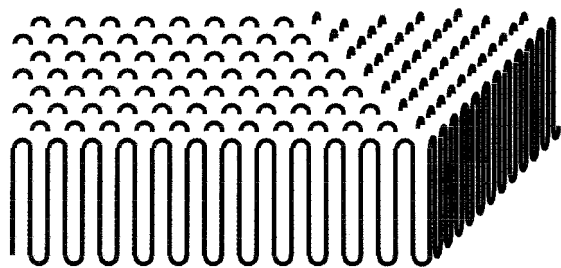


Figure 1. Schematic drawing of a chain-folded polymer crystal.

stable. The order in the schematic structure of the lamella in Figure 1 is certainly idealized, but the exact nature of the fold surface is still unresolved and is a topic of continuing controversy, as are some fundamental aspects of the theory of polymer crystallization. There are a number of reviews and books on the subject.^{1,2,3,4}

Polydispersity has been a greater hindrance to fundamental studies on crystallization and crystal morphology than in most other areas of polymer science. The reason is that, while most polymer properties depend on some power of chain length L , in folded-chain crystals of fold length l it is the length $L - ml$ remaining after m folds that matters in crystallization. If all chains were the same length, nearly 100% crystallinity could be achieved by l adjusting to $l = L/m$, with m being an integer; thus, all chains could end exactly at the crystal surface. However, if a chain is several units shorter than the others, the final incomplete traverse through the crystal layer may leave too large a void; thus, the length $L - ml$ would remain uncrystallized. Polydispersity, which would normally be considered low, may still mean large nonuniformity in $L - ml$. This, in turn, causes the loss of a preferred l -value, reduction in crystallinity, masking of the crystal surface for surface analysis, etc. Furthermore, partial fractionation that occurs on crystallization of polydisperse material makes it difficult to obtain accurately such essential information as crystal growth rate dependence on supercooling and thus find decisive experimental evidence to distinguish between competing crystallization theories. One can approximate monodisperse polymers by using narrow molecular weight fractions. However, the way to achieve truly monodisperse material is to use classical methods of synthetic chemistry rather than polymerization. In the case of polypeptides, it is also possible to resort to biosynthesis using genetically modified bacteria. Monodisperse oligomers with a few tens of chain atoms have been synthesized chemically and studied for many years, most notably n -alkanes, the oligomers of polyethylene (see Sections II.A and II.J), and more recently short oligomers of a number of aromatic polymers.^{5,6} Single-crystal X-ray structures of such oligomers have, e.g., helped in structure determination of their polymer analogues, since polymer single crystals are in general far too small for such analysis.

To be of maximum benefit in studies of crystallization and morphology, monodisperse compounds with chains long enough to fold must be synthesized. Thus

far, this has been achieved with alkanes, alkane-oxyethylene block copolymers, nylon oligomers, and a few sequential oligopeptides. This review will concentrate on studies of monodisperse systems where such exist. Research on narrow molecular weight fractions of polymers will also be covered where data on monodisperse analogues are scarce or absent, notably poly(ethylene oxide). Studies of the crystalline or semicrystalline state of large cyclic oligomers, long-chain branched model compounds, and end-group modified chains are reviewed in addition to those on simple linear chains. Crystallizable di- and tri-block copolymers are covered only partially, to the extent that they impinge on other topics in this article and bear on the general subject of polymer crystallization. The article covers a considerable time span in view of the fact that no review of this kind has been presented in the past. The exception is an early review by Keller in proceedings of a conference which, to the authors' knowledge, have never been published.⁷

II. Lamellar Structure and Chain Conformation

A. Early Studies

Crystalline n -alkanes have been studied for many years as model chain molecules, and their crystal structure,^{8,9,10} crystal growth and morphology,¹¹ melting temperature,^{12,13} chain mobility,¹⁴ conformational defects,^{15,16} self-diffusion,^{17,18} and other properties were extrapolated to represent the crystalline phase of polyethylene. An early comprehensive review of structural and thermodynamic data was presented by Broadhurst.¹⁹ The extrapolation is valid as the orthorhombic subcell of most crystalline n -alkanes is the same as the unit cell of polyethylene. The similarity extends even to the mesomorphic hexagonal high-pressure phase of polyethylene,²⁰ which has its counterpart in the rotator phase in alkanes with up to 40 carbons.^{21,22} Already in 1952, crystals of n -alkanes as long as a hundred C atoms were studied.¹¹ However, the chain length of the alkanes available until 1985 remained insufficient for chain-folding, which limited their usefulness as model polymers.

The first oligomers prepared systematically with increasing molecular weight that crossed the boundary between extended- and folded-chain crystallization were aliphatic oligoamides^{23,24} and oligourethanes.²⁵ Both had large monomer repeat units and could therefore be obtained with comparatively high homologue purity (e.g., 95%). Their lamellar periodicity l , as measured by small-angle X-ray scattering (SAXS), was proportional to the average length of extended chains. However, above a certain molecular weight, l remained constant, which was attributed to the onset of chain folding. This is illustrated in Figure 2. The folding was clearly of the noninteger type (see Section II.C) and the model of molecules following each other as in Figure 3⁷ has been proposed. Similar behavior was also found in a series of polydisperse low molecular weight poly(ethylene oxides) (PEO) samples,²⁶ in contrast to the observations on sharp fractions of this polymer, described next.

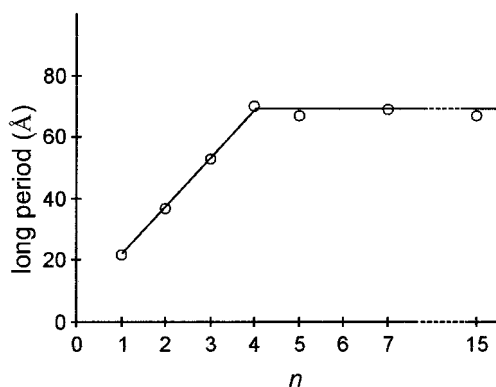


Figure 2. SAXS long period vs number of monomer units n in oligourethane $\text{HO}(\text{CH}_2)_2\text{O}(\text{CH}_2)_2[\text{OCONH}(\text{CH}_2)_6\text{NHCOO}(\text{CH}_2)_2\text{O}(\text{CH}_2)_2]_n\text{OH}$ (after ref 25).

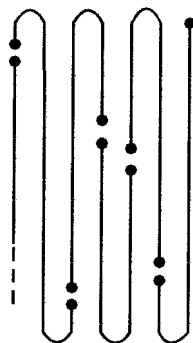


Figure 3. Model proposed to explain the constant l_{SAXS} value for oligourethanes with $\text{DP} > 4$ (after ref 7).

As PEO oligomers could be obtained with narrow molecular weight distribution, their solid state and crystallization kinetics have been studied extensively since early on. Skoulios and co-workers²⁷ found that by crystallizing a fraction with $M_n = 24\,000$ at decreasing crystallization temperatures T_c , the SAXS lamellar periodicity l assumed discrete values corresponding closely to integer fractions of the average chain length L , i.e., $l = L, L/2, L/3$, or $L/4$. Such behavior indicates that the preferred crystallization modes were those which place the chain ends at the surface of the crystalline lamellae. This is in contrast to the situation in polydisperse polymers where l decreases continuously with decreasing T_c , l being proportional to $1/\Delta T$, where $\Delta T = T_m - T_c$, is the supercooling and T_m the melting point.

Many of the important findings from the now classic series of studies by Kovacs and co-workers on narrow PEO fractions have been summarized in refs 28 and 29. Molecular weight fractions were crystallized from the melt in a wide range of supercooling ΔT . Single crystals, large by polymer standards, were grown from the melt at low and moderate ΔT , and revealing experiments were carried out by optical microscopy. They confirmed the quantization of lamellar thickness, a phenomenon which received further support from the observation that melting temperatures also varied in discrete steps. An opinion has existed at the time that integer folding in PEO fractions may be due to the specific nature of the OH end groups and their hydrogen-bonding tendency. We shall return to specific aspects of these studies in subsequent sections.

Chain conform.	E	F2	F3	F4	F5
Paraffin		∩	∩∩	∩∩∩	∩∩∩∩
C102	+				
C150	+	+			
C198	+	+	+		
C246	+	+	+	+	
C294	+	+	+	+	
C390	+	+	+	+	+

Figure 4. Integer folded (IF) forms observed in long n -alkanes $\text{C}_{102}\text{H}_{206}$ through $\text{C}_{390}\text{H}_{782}$. For a given alkane more folds per molecule are obtained with increasing supercooling ΔT (after ref 40).

B. Integer Folded (IF) Forms

The first monodisperse oligomers showing chain folding were long normal alkanes synthesized in 1985 independently by Bidd and Whiting³⁰ and by Lee and Wegner.³¹ Whiting et al. used Wittig coupling in a sequence of chain-doubling steps. Since at each step the product and reactants had a molecular weight ratio of 2:1, it was possible to separate them cleanly and avoid homologue impurities. The method has subsequently been perfected and extended to long alkane derivatives.³²

Crystallization experiments on long alkanes have been performed both from solution and from melt. Many orders of small-angle X-ray diffraction were present due to the high regularity of lamellar stacking. This allowed accurate measurement of lamellar spacing. At the same time the length of straight chain segments was determined by low-frequency Raman spectroscopy using the longitudinal acoustic mode (LAM). While alkane $n\text{-C}_{102}\text{H}_{206}$ could only be obtained in extended-chain form, $n\text{-C}_{150}\text{H}_{302}$ could also be crystallized with chains folded in two (F2, once-folded) from solution or by quenching from melt. With increasing chain length, the maximum number of folds per chain increased, and the longest alkane, $\text{C}_{390}\text{H}_{782}$, could be obtained with $m = 4$ folds, i.e., with chains folded in five ($l = L/5$).³³ The different chain conformations achieved by crystallizing Whiting's alkanes are shown in Figure 4.

In mature crystals the strong preference for integer folding (IF) was indeed confirmed. In solution-grown crystals the relationship $l = L/(m + 1)$, with m an integer, was strictly observed for l measured by both SAXS and LAM. The agreement for l_{SAXS} was to 0.1 nm. For melt-crystallized alkanes, l_{SAXS} had to be corrected for the 35° chain tilt with respect to the layer normal (see Section II.E). These results on alkanes have shown that the preference for integer folding is inherent in monodisperse oligomers and is not due to the specific nature of the end-groups as might have been argued in the case of PEO. In fact it was found subsequently that fractions of methoxy-terminated PEO also exhibit a preference for integer folding.³⁴

The fact that the length of a straight chain segment traversing the crystal (stem length, l_s) is known precisely in IF of a monodisperse oligomer has been used for the calibration of analytical techniques such as Raman LAM spectroscopy and for determining

fundamental polymer parameters such as equilibrium melting point and ultimate elastic modulus of a polymer.

Raman spectra of certain crystalline polymers and their oligomers show a series of identifiable LAM bands in the low-frequency region, corresponding to symmetrical longitudinal backbone vibration modes. In the simplest approach, the stem is considered as a continuous elastic rod, the frequency of the vibration being³⁵

$$\nu_j = \frac{j}{2l_s} \left(\frac{E}{\rho} \right)^{1/2} \quad (1)$$

where E is Young's modulus of the chain, ρ the density, and j the vibration order (only odd orders are Raman active). The fact that LAM frequency is inversely proportional to the straight stem length l_s makes this a valuable technique for studying polymer morphology. Extended chain monodisperse oligomers are ideal for testing eq 1,^{36–38} and finding the value of E , since $l_s = L$. Although eq 1 has been commonly used in the past, weak interlamellar forces result in an upward shift of ν . Thus according to Strobl et al.,³⁹ who studied alkanes C_nH_{2n+2} with $33 \leq n \leq 94$,

$$\nu_j = \frac{2236j}{n-1.6} + \frac{2.2}{j} \quad (2)$$

The associated elastic modulus of polyethylene is $E = 290$ GPa. However, the critical test of eq 2 is in the $l_s \rightarrow \infty$ region. The results for long extended-chain alkanes up to $C_{294}H_{590}$ were at variance with eq 2 and obeyed the simple $\nu_1 \rightarrow \infty 1/n$ law, with $\nu \rightarrow 0$ as $l_s \rightarrow \infty$ and with $E = 350$ GPa.^{40,41} Recent experiments point to end-surface disorder as a possible cause of the discrepancy. In the longest pure alkanes, very slow crystallization from the melt is needed in order to create a highly ordered end-surface; this was found to result in higher ν than the more rapid crystallization.⁴² Furthermore, alkane mixtures give lower ν than pure alkanes. The above discrepancy is thus possibly due to the lack of surface order in the longest alkanes used in previous studies. That surface disorder has a noticeable effect is also borne by the observation by Khoury et al.⁴³ that the LAM frequency of n - $C_{36}H_{74}$ and n - $C_{94}H_{190}$ is affected by end group packing; the effect was attributed to differences in methyl end group interaction.

While the interlamellar forces in n -alkanes are weak and their contribution to the LAM frequencies is small, in systems with strongly interacting chain ends the effect can be very pronounced.⁴⁴ For example, while in n -alkanes, the ratio ν_3/ν_1 is around 2.8, quite close to 3 as expected from eq 1, ν_3/ν_1 is only 2.1–2.3 for monodisperse oligo(oxyethylenes) and PEO fractions.^{45,46} In PEO fractions, this effect makes it difficult to distinguish between LAM-3 of the extended chain conformation and LAM-1 of the once folded chain, and peak assignment must be made with caution. The helical conformation of PEO accounts for its low elastic modulus (25 GPa), as obtained from LAM frequencies.⁴⁷

Linear oligomers have been used extensively in the determination of polymer melting points. The equi-

librium melting temperature of an ideal polymer crystal, though fundamentally important in crystallization, cannot be determined directly. Instead, it is often obtained by extrapolation to infinite chain length of melting points of a series of extended-chain oligomers. Early extrapolations were based on the presumption that both the enthalpy and entropy of fusion were linear in the number of repeat units n per chain.^{48,19} However, in their analysis of melting points of alkanes $C_{11}H_{23}$ to $C_{100}H_{202}$, Flory and Vrij¹² suggested that a nonlinear term $R \ln n$ be included in the entropy of fusion to account for the "unpairing" of chain ends upon melting of the crystal. Their extrapolation leads to a 4 K increase in the equilibrium melting point of polyethylene (from 414.5 to 418.5 K), but the quality of fit was hardly improved compared with previous equations¹⁹ as pointed out by Wunderlich.¹³ The validity of the term $R \ln n$ is supported by studies on PEO fractions,⁴⁹ while evidence for it is not clear in long-chain ketones.⁵⁰

The melting points of long alkanes with $150 < n < 390$ were found to be consistently lower than predicted by Flory's theory.^{31,33} This has been discussed in terms of the premelting effect.⁵¹ Assuming a constant entropy change due to premelting, Carlier et al. found a linear relationship between the melting points T_m of oligomers and the value $(\ln n + C)/n$ where C is a constant.⁵² These authors have carried out extrapolations for polyethylene ($11 < n < 390$), poly(tetrafluoroethylene) ($5 < n < 24$), poly(methyl-eneoxide) ($4 < n < 22$), poly(ethylene oxide), poly(etheretherketones) (PEEK, $1 < n < 4$), and poly(phenylene sulfide) (PPS, $1 < n < 7$). Studies of melting points of folded-chain PEO fractions have shown that, for a given fold length l , the melting point increases with increasing total chain length L , i.e., with increasing number of folds per chain.⁵³ End- and fold-surface free energies for PEO were derived. These parameters were also derived for polyethylene,^{54,55} using melting point data for different IF forms of n -alkanes.³³ Melting points of monodisperse linear and cyclic oligo(oxyethylenes) were found to be in general agreement with the Flory-Vrij expression, provided "segment" and "repeat unit" were appropriately defined.¹²⁶

C. Noninteger Folded (NIF) Form

While mature alkane crystals show a strong tendency for integer folding, when melt crystallization was monitored in real time by SAXS using synchrotron radiation, it was found that below the extended-chain growth temperature region the initial lamellar periodicity l was a noninteger fraction of L , even after correcting for tilt.⁵⁶ It corresponded to a fold length between L and $L/2$ and was dependent on crystallization temperature T_c and time. These "noninteger folded" (NIF) lamellae subsequently transformed isothermally by thickening to extended-chain or, at lower T_c , by "thinning" to once-folded (F2) chain lamellae with hairpin chain conformation. In Figure 5a the real-time SAXS recording of isothermal crystallization of $C_{246}H_{494}$ shows the rapid emergence of NIF marked by the strong first-order peak. This is followed by its demise and concurrent replacement

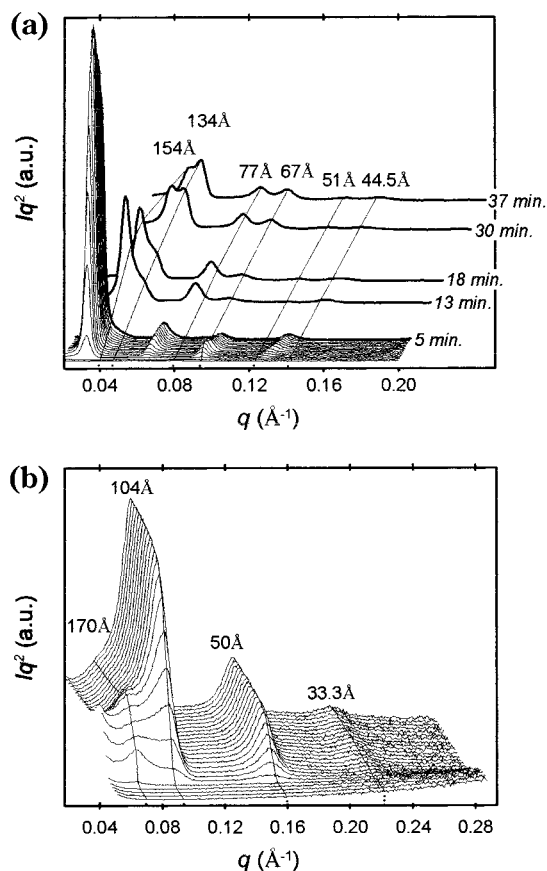


Figure 5. Time evolution of SAXS during isothermal crystallization of (a) *n*-alkane $C_{246}H_{494}$ at $T_c = 111$ °C and (b) branched alkane $C_{96}H_{193}CH(CH_3)C_{94}H_{189}$ at $T_c = 110$ °C from the melt. Abscissa scale is marked in q (in \AA^{-1}) and $d = 2\pi/q$ (in \AA). In panel a, the spectra were recorded sporadically after the first 5 min. Time t is counted from the moment of reaching T_c . In panel b, time frames of 12 s begin from the start of cooling and T_c is reached in frame 4. In panel a, the first-order NIF peak is initially by far the strongest, while in panel b, centered at 170 \AA , it is weak and short-lived (from 59 with permission of American Chemical Society).

by the once-folded form. Subsequently, NIF and its transformation to IF forms were also found in PEO fractions.^{57,58}

The nature of the NIF form, at least in alkanes, has only been understood after electron density profiles normal to the lamellae had been reconstructed using SAXS intensities of a number of diffraction orders.⁵⁹ It turns out that NIF is up to one-third amorphous, with some chains integrally folded in two and others not folded at all but traversing the crystalline layer only once (see Figure 6b). These latter chains are only half-crystalline, with their protruding ends, or cilia, forming the amorphous layer. From the crystalline layer thickness l , determined from the electron density profile, and from $l_{\text{LAM}} = l/2$, determined from time-resolved Raman spectroscopy,⁶¹ it was established that the chains are tilted at 35° to the normal in the crystalline layers.

Compared to the integer F2 form, NIF allows crystals to grow faster since not all chains need attach “correctly”, i.e., with their ends flush with the crystal surface (Figure 6a). However, if the lamella is to grow, nearly half the chains do need to be placed

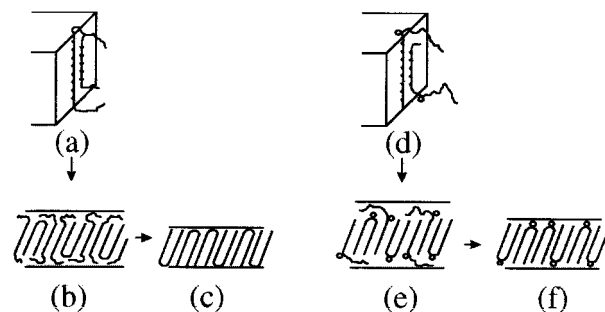


Figure 6. Schematic representation of molecular deposition on the crystal growth face (a, d), the NIF form (b, e), and the F2 form (c, f) for a linear alkane (a–c) and the branched alkane $C_{96}H_{193}CH(CH_3)C_{94}H_{189}$ (d–f). (From 59 with permission of American Chemical Society).

“correctly” and crystallize fully with a fold in the middle. Otherwise the overcrowding at the crystal–amorphous interface, caused by the doubling in cross-section of chains emanating from the crystal,⁶⁰ would build up unsustainably. It is because of this overcrowding effect that lamellar crystals of flexible polymers cannot grow laterally without chain folding. More information on the surface overcrowding effect is provided by studies of alkane mixtures (see Section II.J).

The growth of semicrystalline NIF in preference to that of the highly crystalline F2 form is a typical example of crystallization kinetics controlling polymer morphology. The best known example is, of course, the very fact that thin folded-chain crystals form in preference to the more stable extended-chain crystals.

It is interesting to compare crystallization of a linear alkane with one having a methyl branch in the middle, $C_{96}H_{193}CH(CH_3)C_{94}H_{189}$. There is a strong tendency for methyl branches to be rejected to the lamellar surface and $C_{96}H_{193}CH(CH_3)C_{94}H_{189}$ persistently gives F2 crystals (for more on branched oligomers see Section II.I). Figure 5b shows the evolution of SAXS during isothermal crystallization of the branched alkane. The appearance of the small NIF diffraction peak at $l = 170$ \AA is succeeded immediately by the emergence of the comparatively strong 104 \AA peak and its higher orders attributed to the once-folded form. The rapid NIF \rightarrow F2 transformation can be explained by the fact that here the only successful deposition mode of the first stem (first half) of the molecule is one which places the branch at one lamellar basal surface and the chain end at the other (see Figure 6d). This leaves the molecule with an uncrystallized cilium at one end only, its length being precisely half the chain. Such a cilium is ideally suited to complete a second traverse of the crystal. Thus, although some cilia remain uncrystallized during primary formation of the lamellae, giving rise to the NIF form (Figure 6e), when they subsequently enter the crystal, it is relatively easy for the F2 conformation to be achieved (Figure 6f). In contrast, for a linear alkane in the NIF form, a half-crystallized molecule generally has a cilium at each end; neither of them is long enough to complete a second traverse without rearrangements involving the whole molecule. In the sequence melt \rightarrow NIF \rightarrow

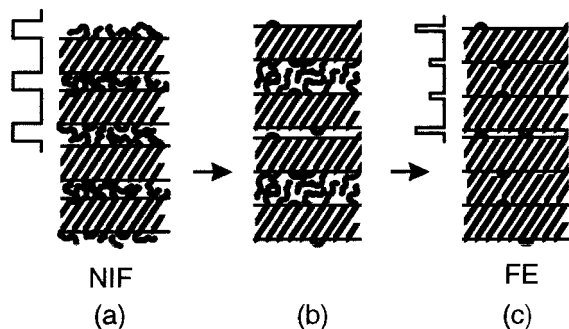


Figure 7. Schematic representation of the transformation from (a) NIF (four layers shown) to (c) mixed folded-extended (FE) forms (two triple layers shown) in long-chain *n*-alkanes with around 200 C atoms. The intermediate stage in panel b should not be taken literally, as the cilia are likely to crystallize simultaneously with their coalescence in the middle layer (from ref 61, by permission of Elsevier Science Publishers).

F2, the melt \rightarrow NIF step is fast but the NIF \rightarrow F2 step (“lamellar thinning”) is slow in linear alkanes. The reverse is true for the branched alkane.

As described, the process of “lamellar thinning”, after NIF formation, consists for most alkanes of the uncrystallized cilia finding their way into the crystal layer (Figure 6, panels b, c, e, f); the overall long period l is reduced gradually while the crystalline thickness l_c remains constant. Recently, however, another more efficient mechanism of NIF transformation has been discovered for *n*-alkanes in the length range of 200 carbons.⁶¹ Instead of folding back into the crystal, the half-crystallized NIF chains translate cooperatively down and up in alternative layers. All cilia emanating from two adjacent crystal layers thus converge in the space between them (see Figure 7b) and crystallize. This results in a triple-layer crystalline superlattice in which once-folded and extended chains are mixed in the outer two sublayers, while the middle layer contains only interdigitated portions of unfolded chains (Figure 7c). The “mixed integer” character of this form has been confirmed by Raman LAM spectroscopy. Similar examples of cooperative lamellar transformations and complex superlattice formation have recently been found in Y-shaped branched alkanes and long alkane mixtures (see Sections II.I and II.J).

Even though the NIF form in PEO fractions behaves in a similar way to that in long alkanes, it is not clear at this stage if it has the same structure. The fact that the oligomers are not monodisperse is partly responsible for this uncertainty. While NIF density profiles have not been reported for PEO, published time-resolved SAXS curves can provide a qualitative clue. Whereas the model of NIF in Figure 7 gives rise to high SAXS intensity which diminishes with the decrease in the amorphous fraction l_a/l , there would be no significant change in intensity upon the NIF \rightarrow IF conversion in the case of the model in Figure 3. This can be seen from the simple general expression for the total small-angle scattering intensity Q for a two-phase lamellar system:⁶²

$$Q = \frac{l_a}{l} \left(1 - \frac{l_a}{l} \right) (\Delta\eta)^2 \quad (3)$$

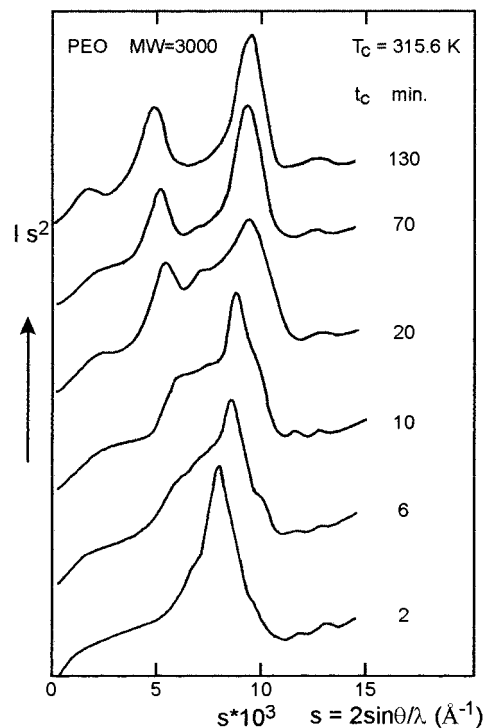


Figure 8. SAXS curves recorded during isothermal crystallization of PEO fraction $M_n = 3000$ at 43 °C. The initial NIF peak (first order) at $t_c = 2$ min gives way to extended and F2 peaks at approximately 5×10^{-3} and $10 \times 10^{-3} \text{ \AA}^{-1}$, respectively (from ref 58 by permission of John Wiley & Sons).

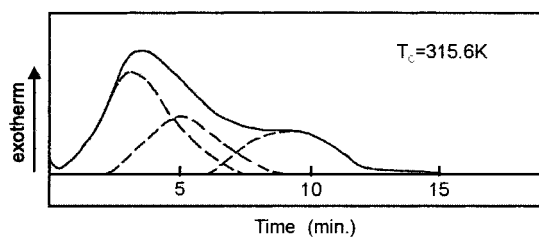


Figure 9. DSC crystallization exotherm for PEO fraction $M_n = 3000$ at 43 °C. Compare with Figure 8 (from ref 58 by permission of John Wiley & Sons).

where $\Delta\eta$ is the crystalline-amorphous electron density difference. Figure 8 shows a series of SAXS traces recorded during isothermal crystallization of a $M_n = 3000$ fraction of PEO at 43 °C, while Figure 9 shows the corresponding DSC exotherm. The overall SAXS intensity does not appear to change much from the first frame (2 min), dominated by the NIF peak, through to the end of the experiment when only the extended and the F2 forms are left. However, at $t = 2$ min crystallization had only just started (Figure 9), while it is complete at $t = 15$ min. This indicates that the initial NIF form scatters considerably more strongly than the IF forms, which would support the two-phase NIF model in Figure 6 and Figure 7. A hybrid model of NIF in PEO has been suggested in the drawing in Figure 10.⁶³ This modifies the model in Figure 3, having chains trail each other through the crystal layer of noninteger thickness, with added loops rather than cilia forming the noncrystalline phase responsible for high SAXS intensity. Electron density reconstruction may help

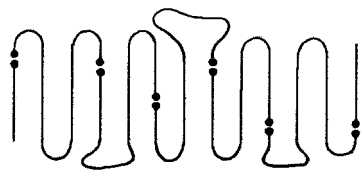


Figure 10. A proposed model of the structure of NIF form in PEO fractions. The black dots represent OH groups (after ref 63).

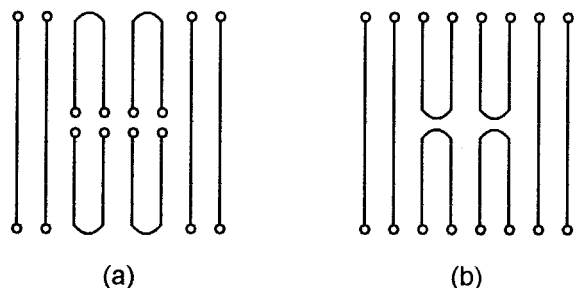


Figure 11. Schematic models of E + F2 crystals of PEO fractions: (a) with internal, (b) with external H-bonds. The models were proposed on the basis of LAM spectra. Model b was preferred (from ref 38 by permission of American Chemical Society).

resolve this structure by establishing the crystalline thickness l_c .

The model of NIF in Figure 6 and Figure 7, as well as that in Figure 10, also appears to be consistent with the "self-decoration" effect observed in PEO fractions,^{28,64} whereby growing chain-folded crystals become decorated by dense overgrowth on their fold surface after quenching. Surface nucleation by cilia, i.e., NIF, is most likely to be responsible, since extended-chain crystals show no such decoration (see Figure 39 and Figure 46).

Raman LAM studies on PEO fractions crystallizing below the F2 melting point consistently show a NIF band with frequency intermediate between those of extended and once-folded chains.^{38,57} This contravenes both the LAM and electron density evidence for the alkanes according to which the length of the straight stem in NIF is always half the chain length. It was found that the noninteger LAM band in PEO transforms with time into F2 and E bands, but no amount of annealing could remove the F2 band completely.⁵⁷ The origin of the discrepancy between the observations on NIF forms in alkanes and PEO is unclear and the structure of NIF in PEO fractions remains essentially unresolved. It ought to be mentioned that LAM in PEO is much more sensitive to end-effects (end-group type, see Section II.G, interlamellar interaction) and intracrystalline packing as compared to alkanes.^{44,65}

The persistence of the F2 LAM band on annealing, without the presence of a SAXS or a DSC melting peak corresponding to F2 lamellae, has led Kim and Krimm³⁸ to propose a tentative model of once-folded chains embedded into an extended-chain lamella (see Figure 11b). A similar structure, proposed in a preceding study³⁶ (Figure 11a) was dismissed on grounds that it would transform easily to the extended chain form.

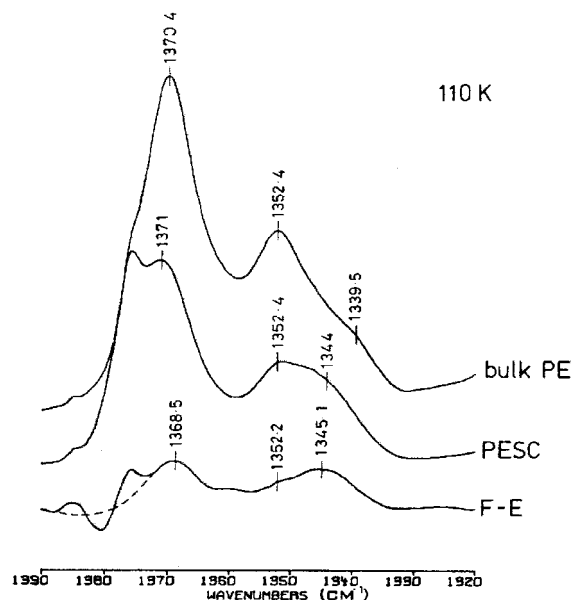


Figure 12. (F-E) Characteristic FTIR spectrum of {110} chain folds in solution-grown single crystals of *n*-alkane $C_{198}H_{398}$ (spectrum of extended-chain crystals subtracted from that of once-folded crystals); (PESC) solution-grown single crystals of polyethylene; (bulk PE); melt-crystallized linear polyethylene. All bands are CH_2 wagging defect modes except the CH_3 band at 1378 cm^{-1} . Spectra recorded at 110 K (from ref 68 by permission of Elsevier Science Publ.)

D. Fold- and End-Surface

The nature of the fold surface of polymer crystals has been a controversial issue for several decades. Models have ranged from the highly ordered, with tight adjacently re-entrant folds (idealized in Figure 1),² to the random re-entry "switchboard" model with loose loops.⁶⁶ One of the reasons for the controversy is the lack of a suitable conformation-sensitive surface technique. However, perhaps a more important reason is the fact that even in solution-grown single crystals an amorphous layer of cilia and probably adsorbed chains covers the fold surface.⁶⁷ Monodisperse long alkane crystals grown from solution in an integer folded form have the advantage of not containing cilia and thus having the fold surface uncovered. This was taken advantage of in recording the IR spectrum of chain folds in crystals of alkane $n-C_{198}H_{398}$.⁶⁸ It was ascertained first by electron microscopy of surface-decorated⁶⁹ crystals used that the folds were predominantly in the {110} planes. The spectrum of extended-chain crystals was subtracted in order to obtain the spectrum of pure folds. In the methylene wagging range, sensitive to conformational defects, the fold spectrum at room temperature was almost indistinguishable from that of amorphous polyethylene, indicating that a range of fold conformations were present. However, at low temperature, the fold spectrum differed considerably from that of bulk polyethylene (see Figure 12). It was dominated by bands at 1368 and 1345 cm^{-1} , the former being due to *gtg* defects and the latter appearing to be specific to regular {110} folds. Significantly, the prominent *gg* band at 1352 cm^{-1} almost vanished at low temperature. The 1345 cm^{-1} band

Table 1. Parameters of Inter-crystalline Layer for Extended (E) and Once-Folded (F2) Chain Long Alkanes Derived from SAXS

sample	form	temp (°C)	electron deficiency per unit area of interlayer, κ (electron \AA^{-2}) ^a	width of interlayer from κ assuming noncrystalline density = 0.85 g cm ⁻³ (\AA) ^a	integral width of interlayer (I_a) (from Fourier synthesis) (\AA)
C ₁₉₄ H ₃₉₀ or C ₁₉₈ H ₃₉₈ melt-crystallized	E	rt	0.66	13	15 ^b
		120			26 ^b
solution-cryst	F2	rt	0.40	8	17 ^c
C ₂₄₆ H ₄₉₄ melt-crystallized	E	rt	0.66	13	26 ^b
		122			32 ^b
F2	F2	rt	0.73	14.5	18 ^c
linear polyethylene melt-crystallized		rt	2.4	48	

^a Using absolute intensity SAXS data.⁷⁶ ^b From ref 75. ^c From ref 77.

also appears as a shoulder in the low-temperature spectrum of polyethylene single crystals, but not in that of bulk polyethylene. A band at 1345 cm⁻¹ has been suggested to represent tight folds by previous studies of polyethylene using curve deconvolution.^{70,71}

The observed high conformational uniformity, i.e., "tight" folds, could not have been attained at low-temperature had the folds not been connecting adjacent stems in the first instance. A switchboard-type fold surface would not have produced the spectrum at the bottom of Figure 12, but rather one like that at the top of the figure.

A band of moderate intensity has been observed at 1080 cm⁻¹ in the Raman spectrum of once-folded solution-crystallized *n*-alkane C₁₆₈H₃₃₈.⁷² This spectral region is associated with C–C stretching vibrations of methylene sequences containing gauche bonds. Extended-chain shorter alkanes (*n*-C₄₈H₉₈, *n*-C₇₂H₁₄₆) did not show this band. The 1080 cm⁻¹ band is also observed in semicrystalline polyethylene.⁷³ Low-temperature spectra were not reported.

Information on the density profile across the intercrystalline chain-fold or chain-end layer can be obtained from SAXS intensities.^{74,75} Table 1 gives experimental data describing the state of the lamellar surface layer in E and F2 forms of two long alkanes.^{75,76,77} The electron density profile normal to the layer surface is proportional to the mass density profile in the case of alkanes. This has a minimum as one crosses the inter-crystalline gap. The integral of that minimum (κ) and its integral width (I_a) are listed. As can be seen, solution-grown crystals have the smallest inter-crystalline gap (κ), although it is spread over a width of 17 \AA (I_a), hence the gap is shallow. Melt-crystallized alkanes have a similar I_a , but the gap is deeper. The gaps for E and F2 forms are similar, but the relative contribution of the interlayer is of course twice as large in the F2 form. In comparison, κ for polydisperse polyethylene is much greater.

As mentioned earlier, in addition to *n*-alkanes, pure monodisperse nylon 6⁷⁸ and nylon 6,6⁷⁹ oligomers have also been successfully synthesized with sufficient length to form chain-folded crystals. Once-folded chain crystals of nylon 6 nonamer and decamer,^{80,81} and twice-folded crystals of nylon 6 17-mer⁸² have been obtained from solution and studied by means of X-ray and electron microscopy and diffrac-

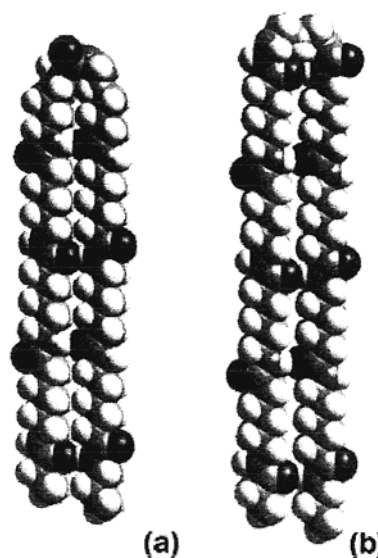


Figure 13. A once-folded conformation of nylon 6 nonamer with an amide fold (a) and of decamer with an alkane fold (b). (After ref 80).

tion. Nylon 6 oligomers were found capable of forming alkane folds or amide folds, although it was thought previously that amide folds could only be found in nylon 4⁸³ and nylon 4,6.⁸⁴ Symmetrical once-folded conformations of 9-mer and 10-mer, consistent with the measured SAXS long spacings, have different fold types (Figure 13). The crystal subcell is that of nylon 6 α -structure with hydrogen-bonded sheets. On the basis of molecular mechanics calculation aided by simulation, it was concluded that the folds were in the plane of the sheets. In 12-amide and 16-amide nylon 6,6, only once-folded crystals have been obtained.⁸⁵ Temperature-induced structural changes in crystals of monodisperse nylon 6 and nylon 6,6, such as unfolding, intersheet shear, and orthorhombic-pseudohexagonal transition, have also been studied.⁸⁵

Several monodisperse model proteins with repeating sequences of amino acids have been biosynthesized by the recombinant DNA technique and have had their structure studied.⁸⁶ Multigram quantities were produced in pilot fermentators. Thus, poly(L-alanyl-glycine), poly(AG), with alternating alanyl and glycy units, was prepared with two different chain lengths: (AG)₆₄ and (AG)₂₄₀.⁸⁷ Structural studies were

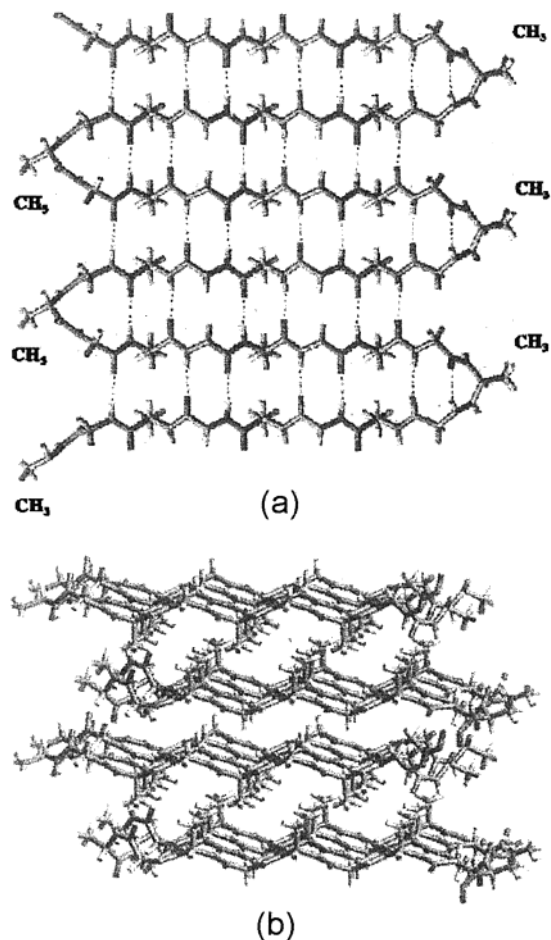


Figure 14. (a) Top view of a single antiparallel β -sheet of biosynthesized monodisperse poly(alanyl-glycine). Fold length is commensurate with the octapeptide periodicity. Vertical dotted lines indicate H-bonds. (b) Arrangement of β -sheets into 3-D crystal. Sheets lie horizontally. Energy-minimized model refined using X-ray data (from ref 87, by permission of the American Chemical Society).

carried out on pressed partially oriented crystal mats. The structure was found to be similar, but not identical to that found previously in oriented films of synthetic poly(AG) and fibers of corresponding silk fibroin.^{88,89} The structure was that of antiparallel β -sheets, i.e., layers of internally hydrogen-bonded chains in the 2_1 zigzag conformation, with adjacent chains oriented in opposite directions. In silk II, extended antiparallel chains form stacked strands of β -sheets. In biosynthesized (AG)₆₄, the chains are folded. The antiparallel arrangement is compatible with adjacently re-entrant chain folding. In poly(AG) a fold occurs after every 8 amino acids, as determined from the observed X-ray spacing of 32 Å. The 32-Å-wide β -sheets were stacked to form a 3-D crystal, as suggested in the computer model in Figure 14. Note that the individual β -sheets are polar as the methyl groups not involved in the folds are all either above or below the plane of the sheet.

The following polypeptides of the type [(AG)_xEG]_n (*E* = glutamic acid) have also been prepared by biosynthesis: *x* = 3, *n* = 36; *x* = 4, *n* = 28; *x* = 5, *n* = 20; and *x* = 6, *n* = 14.^{86b,90} Structural studies were carried out on [(AG)₃EG]₃₆. The basic pattern of antiparallel β -sheets of folded chains forming 3-D

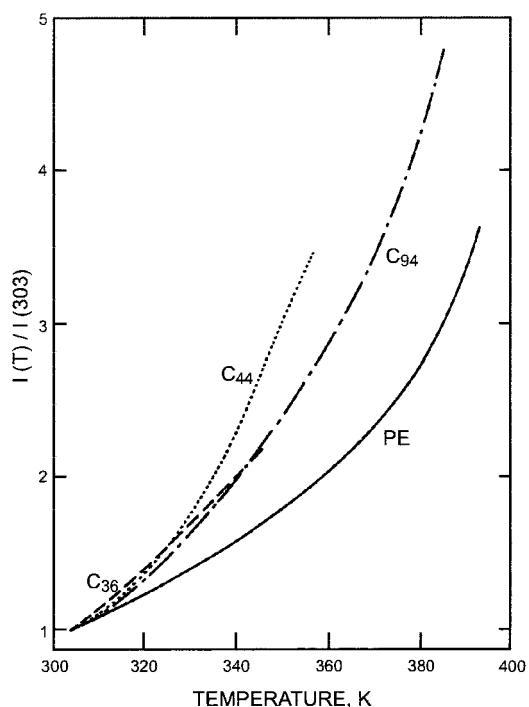


Figure 15. Temperature dependence of relative intensities of the first order (001) small-angle X-ray diffraction for *n*-alkanes C₃₆H₇₄, C₄₄H₉₀, C₉₄H₁₉₀, and linear polyethylene (from ref 93 by permission of National Institute of Standards and Technology).

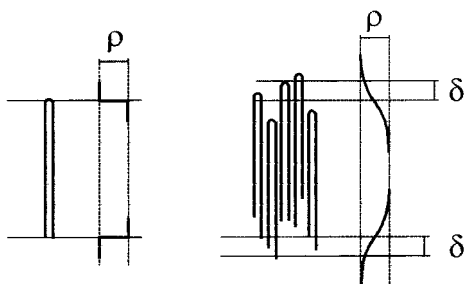
crystals was present here too. The measured fold length of 32 Å was found to be commensurate with the length of the chemical repeat of eight amino acids. The fold occurred at the glutamic acid position, so that the layers had carboxylic groups on their surface.^{91a} A similar structure was also found in a related polypeptide which had the alternative tri-(alanyl-glycyl) segments reversed, i.e., [(AG)₃EG-(GA)₃EG]₁₀.^{91b} In both cases, the X-ray data were compatible with molecular models containing the so-called γ -fold. A γ -fold encompasses two planar amide groups, whereas a β -fold contains only one amide group. Most globular proteins contain γ -folds. Since γ -folds are found in both poly[(AG)₃EG] and poly[(AG)₃EG-(GA)₃EG], it was concluded that interaction between sheets is not the primary factor determining the fold type.

Returning to long *n*-alkanes, it was found that when the once-folded crystalline C₁₉₈H₃₉₈ is heated from 110 K to room temperature, the IR spectrum of chain folds changes from that in Figure 12 (bottom) to one that is not very different from that of amorphous polyethylene.⁶⁸ This indicates reversible conformational disordering with increasing temperature. While remaining adjacently re-entrant, the loops become looser. Reversible thermal disordering of the fold-surface in long alkanes is particularly pronounced close to the melting point.^{40,92}

A similar reversible thermal disordering of the surface layer has also been observed in extended-chain alkanes, starting from the early work on *n*-C₉₄H₁₉₀,⁹³ where the effect has been compared to the premelting phenomenon in polymers.⁹⁴ This is illustrated in Figure 15 where the temperature-

Table 2. Relative Intensities of the "Crystalline" Signal in the Magic-Angle Spinning ^{13}C NMR Spectra of Alkane $n\text{-C}_{168}\text{H}_{338}$ (ref 95)

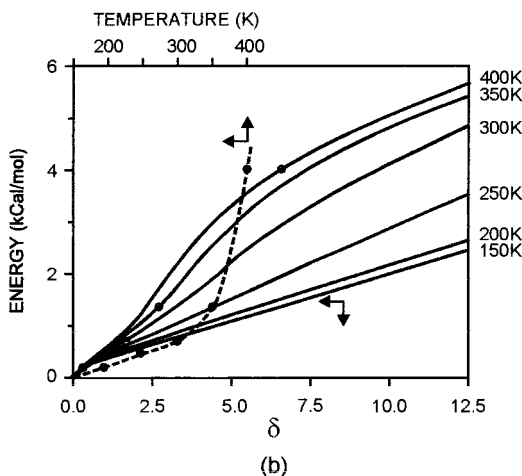
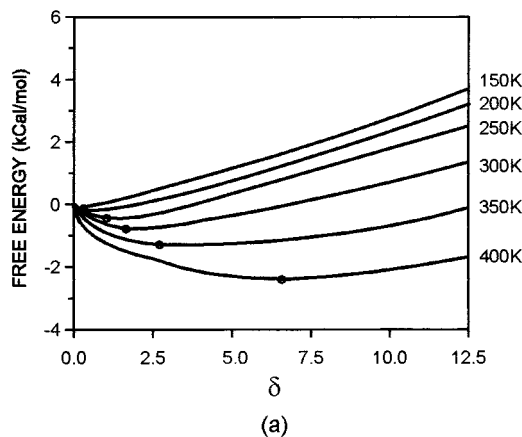
T ($^{\circ}\text{C}$)	internal CH_2	$\alpha\text{-CH}_2$	CH_3
27	0.96 ± 0.05	0.87 ± 0.05	0.79 ± 0.1
87	0.92 ± 0.05	0.63 ± 0.1	0.42 ± 0.1

**Figure 16.** Model used to calculate equilibrium surface disorder in once-folded chain crystals of n -alkanes. Left: complete order. ρ = density (after ref 40).

induced increase in SAXS intensity for extended-chain alkanes and polyethylene are compared. The close relationship between the "noncrystalline fraction" l_a/l and SAXS intensity is evident from eq 3. While in relative terms the intensity increase for polyethylene is the smallest, in absolute terms it is in fact the largest. Table 1 shows the increase in the interlayer widths between room temperature and close to the melting point for extended-chain $\text{C}_{194}\text{H}_{390}$ and $\text{C}_{246}\text{H}_{494}$.

Solid-state ^{13}C NMR experiments on extended-chain $n\text{-C}_{168}\text{H}_{338}$ have shown the strong reversible thermal disordering of chain ends very clearly.⁹⁵ The methyl and α -methylene signals are clearly distinguished from those of inner methylenes; the respective "crystalline" (all-trans) signals are at 16.1, 25.7, and 33.6 ppm, while their "amorphous" (conformationally averaged) counterparts are at 15.5, 24.2, and 31.5 ppm. The relative intensities of the "crystalline" component are shown in Table 2 for 27 and 87 $^{\circ}\text{C}$.

The problem of smooth vs rough surface in a crystal of once-folded alkane has been treated quantitatively.⁴⁰ The method is similar and somewhat simpler for extended chains. The calculation was based on the model in Figure 16. In the figure on the left, l is exactly equal to $L/2$. This allows only two configurations of the molecule: hairpin up and hairpin down (only one is shown in Figure 16). However, if the surface is allowed to be rough, many more configurations become available, as shown on the right. A self-consistent mean field approach was adopted where the interaction potential profile ψ was iteratively matched against the density profile ρ . ψ takes the form of the error function whose width is defined by the standard deviation δ (step function with $\delta = 0$ in the extreme case on the left). Protruding ends were allowed rotational isomeric freedom while the folds were kept tight in this simple model. Standard thermodynamic parameters for polyethylene were used and the resulting free energies vs δ are plotted in Figure 17a. Smooth surface ($\delta = 0$) is favored only below ca. 200 K, the minimum in free energy moving to larger δ (increased roughness) with increasing

**Figure 17.** Molecular free energies (a) and internal energies (b) vs surface roughness parameter δ at different temperatures for once-folded alkane crystal, using the model in Figure 16. Circles mark the free energy minima. The dashed line shows the temperature dependence of equilibrium energy (after ref 40).

temperature. The corresponding energies are shown in Figure 17b, the dashed curve delineating the temperature dependence of the equilibrium state energy. The premelting, or surface roughening, is evident. The dashed curve in Figure 17b should be compared to the temperature dependence of SAXS intensity (Figure 15 and ref 92) and of enthalpy (see Figure 5a in ref 92).

More about the fold surface can be learned from studies of cyclic compounds (see Section II.F).

E. Chain Tilt

Closely associated with lamellar surface disorder is the phenomenon of chain tilt. In many crystalline polymers, chains are often tilted relative to the layer normal. In polyethylene, this leads, e.g., to the "hollow pyramid" shape of solution-grown single crystals.¹ Further, chain tilt is believed to be responsible for lamellar twist in melt-crystallized spherulites.^{96,97} The development of tilt is associated with crystallization or annealing at high temperatures. Thus, e.g., perpendicular-chain lamellar morphology in rolled polyethylene transforms into "parquet-floor" morphology on annealing.⁹⁸ Crystal lamellae with tilted chains are obtained at high T_c from the

melt.^{99,100} In solution-grown crystals of long alkanes, whether folded or extended, the chains are perpendicular, while in those grown from melt, chains are tilted.^{33,93} As in polyethylene, the difference has been associated with T_c being lower in the former case. In polyethylene and long alkanes the tilt is usually 35 degrees, which means that the basal plane is {201} instead of {001} as in the case of perpendicular chains. The {201} tilt arises when each consecutive chain along the a -axis is shifted by one lattice period in the chain direction. Such tilt allows chain ends and folds an increased surface area, by a factor of $1/(\cos 35^\circ)$, while maintaining the crystallographic packing of the rest of the chain intact.¹⁰¹

In apparent agreement with the behavior of polyethylene, shorter n -alkanes crystallize with perpendicular chains as long as T_c is below ca. 60–70 °C.⁸ This is true for odd-numbered alkanes; even-numbered ones display a more complex behavior due to molecular symmetry.¹⁹ At higher temperatures in alkanes such as $C_{33}H_{68}$, a {h01} tilted form is brought about through one or several discrete transitions.¹⁰ In this case, tilt is associated with equilibrium surface disorder, and the absence of tilt with high end-group order. When perpendicular-chain solution-crystallized n -alkanes with more than ca. 50 carbons are heated, chain tilt is introduced gradually. Up to $C_{94}H_{190}$ crystals melt before a tilt of 35° is reached,^{93,102} whereas for alkanes $C_{198}H_{398}$ and longer, the 35° tilt angle is attained, remaining constant until the melting point.¹⁰³ The change is mostly irreversible, i.e., the tilt remains on cooling, which is also often the case with shorter alkanes.

While the lack of tilt in alkanes such as $C_{33}H_{68}$ is identified with high surface order, in polyethylene, it was attributed to a rough disordered surface.^{97,104} Experiments with a recently synthesized¹⁰⁵ end-deuterated long alkane, $C_{12}D_{25}C_{192}H_{384}C_{12}D_{25}$, have provided direct proof that the latter is indeed the case for long chains.¹⁰³ As expected, solution-grown extended-chain crystals have perpendicular chains which gradually tilt to 35° with increasing temperature, as determined by SAXS. However, parallel IR spectroscopy experiments reveal that, instead of increasing in disorder, the crystal surface becomes more ordered at higher temperatures. At all times, crystal interior is more ordered than the surface, but internal order improves only marginally on annealing. The above assertions are evident from the temperature dependence of CH_2 and CD_2 bending modes, shown respectively in panels a and b of Figure 18. In ordered orthorhombic crystals of pure H or D species, these bands are well-resolved doublets due to crystal field (Davydov) splitting. The reduced CD_2 splitting indicates positional or orientational disorder of the deuterated surface layer. Since isolated or amorphous chains show no splitting, the singlet component around 1089 cm^{-1} in the unannealed (25 °C) sample is attributed to excursions of the $C_{12}D_{25}$ group outside the crystal or inside the hydrogenous layer. With increasing temperature, these excursions disappear (Figure 18b).

The above evidence suggests that low-temperature solution crystallization produces a high degree of

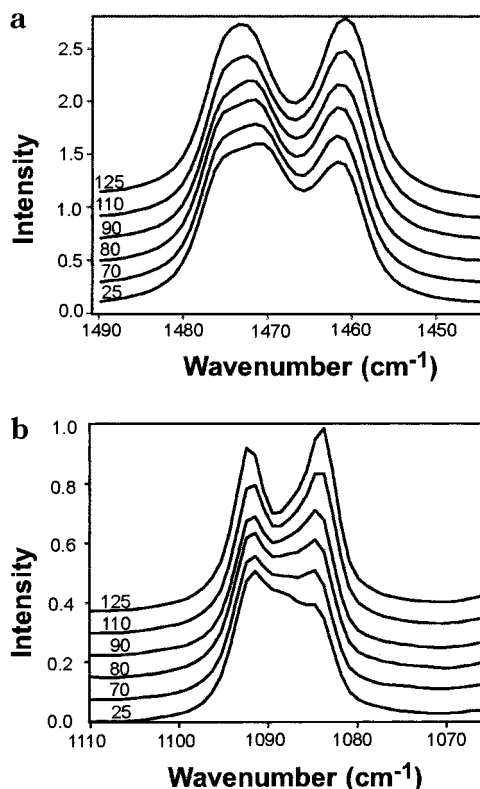


Figure 18. (a) CH_2 and (b) CD_2 deformation bands in the IR spectrum of extended-chain solution-grown crystals of end-labeled n -alkane $C_{12}D_{25}C_{192}H_{384}C_{12}D_{25}$. The sample was annealed at the temperatures indicated (in °C) and the spectra recorded at 110 K (from ref 103).

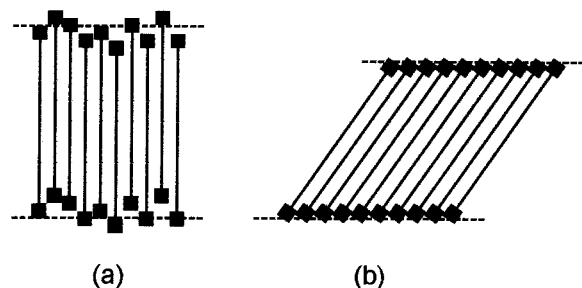


Figure 19. Schematic representation of deuterium end-labeled chains in a crystal as-grown from solution (a) and after annealing (b). The end-group disorder in panel a causes the reduction in CD band splitting in Figure 18b (from ref 103).

translational disorder with randomly staggered chain ends (see Figure 19a). With increasing temperature and mobility, this frozen-in disorder is reduced as uniform stagger with chain tilt replaces the random stagger (Figure 19b). Further support is provided by recent experiments which show that, where it was possible to melt-crystallize extended-chain long alkanes at a high supercooling, perpendicular chains were obtained; these would tilt on subsequent annealing.¹⁰⁶ In light of the above evidence, the model of “buried folds”, i.e., randomly staggered folds, which has been invoked in the past as a possible solution to the surface overcrowding problem,¹⁰⁷ merits attention in the case of crystals grown from melt or solution at low temperatures. The experiments on $C_{12}D_{25}C_{192}H_{384}C_{12}D_{25}$ show that, once annealed, the crystals retain tilted chains, with subsequent heating

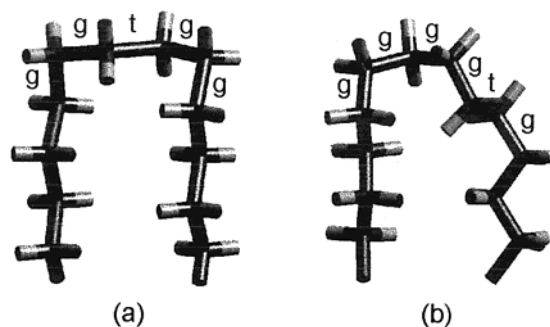


Figure 20. (a) Structure of the chain fold in crystalline monoclinic cycloalkane $c\text{-(CH}_2\text{)}_{34}$, representative of the $\{100\}$ fold in polyethylene (after ref 109); (b) calculated minimum energy conformation of a $\{110\}$ chain fold in orthorhombic polyethylene (after ref 116).

and cooling causing only reversible changes in surface disorder, in agreement with the ideas discussed in the preceding section.

The observation that in polyethylene crystals lateral faces with perpendicular chains grow faster than those with tilted chains^{96,97} is in agreement with the above link between orthogonality and high kinetically induced surface disorder. A parallel situation exists in shorter even-numbered n -alkanes with 28 or more carbons, where a form with perpendicular chains and comparatively rough surface results from rapid melt crystallization, despite the stable structure having smooth $\{011\}$ tilted basal planes.¹⁹ Thus, the only case where orthogonality is due to a highly ordered surface appears to be that of odd-numbered shorter alkanes.^{8,10}

A new crystal structure with tilted chains has recently been found in pentamer of nylon-6 and nylon-8, termed λ -phase.¹⁰⁸ Molecules are in the all-trans conformation and hydrogen bond to antiparallel neighbors to form the usual nylon 6 hydrogen-bonded sheets. However, in this structure, the sheets stack with progressive c -axis shear, and consequently, the molecular layer thickness is noticeably reduced.

F. Cyclic Oligomers

Large cyclic alkanes crystallize as collapsed rings consisting of two straight stems linked by two folds,^{109–111} (cf. Figure 21a). For this reason they have been studied as model folded polyethylene chains. Cycloalkanes up to $(\text{CH}_2)_{96}$ were synthesized by Schill et al.¹¹² and up to $c\text{-(CH}_2\text{)}_{288}$ by Lee and Wegner.³¹ It has been reported that cycloalkanes up to $c\text{-(CH}_2\text{)}_{48}$ are monoclinic, while $c\text{-(CH}_2\text{)}_{72}$ and $c\text{-(CH}_2\text{)}_{96}$ show a mixture of monoclinic and orthorhombic modifications, depending on crystallization conditions.^{72,111} The large ring $c\text{-(CH}_2\text{)}_{144}$ was always orthorhombic, irrespective of crystallization conditions.⁷² Orthorhombic refers here to the subcell, involving only four CH_2 groups; this cell is the same as that in long linear alkanes and polyethylene.

In monoclinic cycloalkanes, unlike in the orthorhombic ones, the zigzag planes of the two stems are parallel to each other (see Figure 20a). The folds in monoclinic cycloalkanes may therefore be representative of polyethylene folds lying in the $\{100\}$ plane,

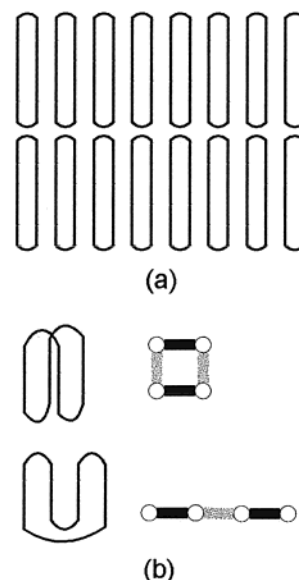


Figure 21. (a) Packing of collapsed rings into crystalline layers; (b) Side and top view of two proposed possible conformations of the folded large cyclic PEO $M_n = 10\,000$ (schematic, from ref 122 by permission of American Chemical Society).

i.e., connecting adjacent stems along the crystallographic b -axis. Such folds are expected primarily in melt-grown polyethylene crystals, where $\{100\}$ growth face is dominant, but not in the rhombic solution-grown crystals where $\{110\}$ folds prevail.¹¹³ In the orthorhombic form, the zigzag planes of the two cycloalkane stems are nearly perpendicular to each other, rather than parallel, and the folds in orthorhombic cycloalkanes may therefore be representative of $\{110\}$ folds in polyethylene (Figure 20b).

Using atomic force microscopy (AFM), lamellar surface of normal and cyclic alkanes $\text{C}_{33}\text{H}_{68}$, $\text{C}_{36}\text{H}_{74}$, $(\text{CH}_2)_{48}$, and $(\text{CH}_2)_{72}$ was examined to atomic scale.¹¹⁴ In the cycloalkanes, the observed images are consistent with adjacent re-entry $\{100\}$ folds in a monoclinic crystal structure.

Room-temperature IR spectra of monoclinic cycloalkanes $(\text{CH}_2)_n$ with $30 < n < 96$ show three bands whose intensity increases as $1/n$, associating them in some ways with the fold.¹¹⁵ These are the 1344 cm^{-1} CH wagging band, already discussed in Section II.D, as well as bands at 1442 and 700 cm^{-1} , presumably CH bending and CH rocking. In melt-crystallized $c\text{-(CH}_2\text{)}_{72}$ and $c\text{-(CH}_2\text{)}_{96}$, which contain an orthorhombic fraction, bands at 1368 cm^{-1} and around 1300 cm^{-1} are also seen, which signifies the presence of gtg defects; the gg band at 1352 cm^{-1} is also present. These results can be rationalized by considering the minimum energy tight fold models: a $ggtgg$ conformation for a $\{100\}$ fold (monoclinic cycloalkanes) and possibly a $gtggg^*g^*$ for a $\{110\}$ fold [orthorhombic cycloalkanes (see Figure 20b)].¹¹⁶ The observed spectra could be understood assuming (a) that the $1342\text{--}1344\text{ cm}^{-1}$ band represents strained gg sequences [monoclinic cycloalkanes and once-folded orthorhombic n -alkanes at low-temperatures (see Section II.D)], and (b) that the 1352 cm^{-1} band represents relaxed gg sequences (orthorhombic once-

folded *n*-alkanes and cycloalkanes at room temperature). Low-temperature spectra of cycloalkanes have not been reported. The calculated energy of a model {110} fold (20.4 kJ/mol) is somewhat higher than that of a {100} fold (16.3 kJ/mol).¹¹⁵ This is consistent with the smaller rings being monoclinic and larger rings orthorhombic. It would appear that stem packing favors the orthorhombic form while folds favor the monoclinic form.

A detailed solid-state ¹³C NMR study on *c*-(CH₂)₁₂, *c*-(CH₂)₂₄, and *c*-(CH₂)₃₆ has been carried out resulting in the assignment of chemical shifts for a number of rotational isomeric sequences in alkanes.¹¹⁷ Chemical shifts for carbons at the center of sequences *gtgg*, *gttg*, *ggtt*, *tggt*, *gttt*, and *tttt* were identified. The assignments were based on low temperature spectra, since at higher temperatures the cycloalkanes investigated transform into highly conformationally disordered crystals with a pseudo-hexagonal structure.^{118,119} In terms of enthalpy and entropy, as well as number of nonplanar conformers, this “mesophase” is closer to the melt than to the ordered crystal. It has therefore been compared to the high-pressure hexagonal mesophase in polyethylene, rather than to the “rotator” phase in linear alkanes with $n \leq 40$.¹²⁰

Even in the largest cyclic alkane synthesized, *c*-(CH₂)₂₈₈, only the “extended” ring conformation has been observed, i.e., the two stems constituting the collapsed ring did not fold further.³¹

Cyclic PEO has been prepared in two ways: (a) with narrow PEO fractions as starting material, using ring closure Williamson reaction^{121,122} and (b) as monodisperse rings, effectively large unsubstituted crown ethers.^{123–126} The largest monodisperse ring prepared and used in crystallization studies was *c*-E₂₇ (E = CH₂CH₂O), or 81-crown-27. In the latter case, the two stems of the collapsed ring were found to have the same helical *tgt* conformation and the same monoclinic subcell as linear PEO chains.¹²⁵ In contrast, smaller rings show a different crystal structure.¹²⁴ The boundary was found to lie between *c*-E₁₆ and *c*-E₁₈.¹²⁶ The melting points of the ring compounds were significantly higher than those of their linear analogues, an effect attributed to a decreased melting entropy.

Rings prepared from commercial PEO fractions had M_n up to 10000 (equivalent to *c*-E₂₂₇).¹²² SAXS and Raman LAM measurements showed that for $M_n = 6000$ such cyclic polymers crystallize as collapsed rings forming layers, as in the case of the large crown ethers and cycloalkanes (see Figure 21a). However, the cyclic polymer of $M_n = 10\,000$ crystallized in a folded conformation when cooled from its melt at moderate rates. That is to say, each stem of the collapsed ring was folded again in two (see Figure 21b). When the $M_n = 10\,000$ sample was crystallized slowly at a high temperature, the conformation of the extended collapsed ring (Figure 21a) was obtained.

A Raman study has shown that LAM-1 frequencies of cyclic PEOs in the range $1000 < M_n < 3000$ are only 1.8 times higher than those of their linear counterparts.¹²⁷ This is in contrast with cycloalkanes, where the LAM-1 frequency of *c*-(CH₂)_{*n*} is nearly exactly twice that of linear C_{*n*}H_{2*n*+2}.¹²⁸

Small ring oligomers of several other polymers have been synthesized, and their crystal structures determined. Thus, relevant to the industrially important cyclic impurities in poly(ethylene terephthalate) (PET), the structures of the low-temperature¹²⁹ and the high-temperature¹³⁰ modifications of cyclic PET trimer have been determined. The structure of cyclic dimer of poly(butylene terephthalate) (PBT) has also been determined¹³¹ in order to help understand a mechanically induced polymorphic transition in the parent polymer. Limited crystallization work has been done on the otherwise extensively studied cyclic oligosiloxanes;¹³² the object was “cold crystallization” near the glass transition temperature.

Cyclic main-chain liquid crystal oligomers have been shown to display a number of crystalline polymorphs in addition to smectic and nematic phases.¹³³ These collapsed rings have rigid mesogens in their “stems” while folds form selectively in the flexible spacer. Significant difference between even and odd-membered rings are seen, particularly where the flexible spacer is short.

G. Oligomers with Specific Endgroups

Prior to the synthesis of long *n*-alkanes in 1985, the narrowest molecular weight distribution achieved in paraffinoid chain systems in the 100–400 C-atom range was α,ω -dicarboxylic acids produced by selective oxidation of solution-grown polyethylene single crystals. Nitric acid or ozone treatments¹³⁴ were applied to remove the fold layer, and the length of the remaining alkanoid diacid was determined by the thickness of the original crystalline layer; this, in turn, could be controlled by the choice of crystallization or annealing temperature. The carboxylic end groups have also been reduced, resulting first in α,ω -dibromoalkanes and, finally, alkanes. While crystallization studies on alkanes thus produced have not been reported, both the long diacids and dibromides showed only continuous change of long spacing with crystallization temperature.¹³⁴

Most linear oligomers can be regarded as having “special” end-groups, and as stated at the beginning, one of the reasons for synthesising long alkanes was the similarity of end groups with the bulk of the chain. In a number of studies of PEO fractions, which are normally OH-terminated, methoxy-terminated equivalents (MPEO) were also examined for comparison. Thus, it was found that crystallization is more rapid in MPEO compared to that in PEO and that the same is true for subsequent transformation of NIF into IF forms.³⁴ OH groups show a degree of hydrogen bonding, as evidenced by IR spectroscopy. The self-diffusion coefficient of MPEO in the melt was found by spin-echo NMR measurements to be higher, by a factor of 1.17, than that of PEO, although the activation energies were the same.

There has been some evidence from TEM¹³⁵ and Raman⁴⁵ that hydroxy-terminated PEO fractions form double-layer crystals, but doubts have been expressed subsequently.³⁸ End-group interaction in low-molecular weight PEO fractions certainly has a pronounced effect on LAM frequency. The following two linear relationships were found between the

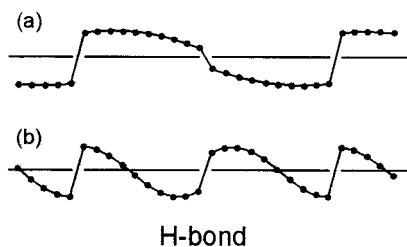


Figure 22. Schematic representation of the vibrational displacement describing the first (a) and the second (b) LAM modes for a molecular dimer in α -methyl- ω -hydroxy-[oligo(oxyethylenes)]. Longitudinal displacement is presented as transverse (from ref 47 by permission of American Chemical Society).

frequency of LAM-1 mode (in cm^{-1}) and reciprocal chain length (in \AA^{-1}):³⁸

$$\text{PEO: } \nu_1 = 1161.1 L^{-1}$$

$$\text{MPEO: } \nu_1 = 1094.7 L^{-1}$$

The case for double layer formation in PEO-type oligomers has been made in a series of monodisperse α -methyl- ω -hydroxy[oligo(oxyethylenes)], or $\text{C}_1\text{E}_p\text{OH}$, where p is the number of oxyethylene units.⁴⁷ The authors have applied the dynamic model by Minoni and Zerbi⁴⁴ to describe the two strongest LAM peaks observed in Raman spectra. These correspond to what can be described as first and second modes of a dimer (see Figure 22).

When a series of OH-terminated monodisperse oligo(oxyethylenes) and PEO fractions were compared, it was found that in the former case H-bonding has a considerably stronger effect in increasing the LAM-1 frequency relative to methoxy terminated chains.¹²¹ This stronger H-bonding was attributed to the regularity of the end-surface in monodisperse compounds.

Short-chain fatty acids are well-known to crystallize as double layers due to dimerization by hydrogen bonding.¹³⁶ Recently, however, bilayer crystallization has been demonstrated in a very long-chain n -alkanoic acid, $\text{C}_{191}\text{H}_{393}\text{COOH}$.¹³⁷ Figure 23 shows a series of SAXS curves recorded during slow cooling of the acid from the melt. The traces in the front represent the bilayer phase crystallized at the highest temperature. Odd diffraction orders of the 410 \AA periodicity are dominant, which is compatible with the electron density profile in Figure 24a, with carboxylic layer maxima and methyl layer minima. Below 129 $^\circ\text{C}$, crystallization switches to producing 205- \AA -thick monolayers, as indicated by the apparent intensification of even-order reflections. In the monolayer form, carboxylic groups are evenly distributed between either surface of the crystal layer (see Figure 24b). IR spectra show that most carboxylic groups are H-bonded both below and above the melting point.¹³⁸ $\text{C}_{191}\text{H}_{393}\text{COOH}$ dimers thus act as supramolecular chains of twice their molecular length. Crystallized in bilayers and monolayers, they can be considered, respectively, as extended and once-folded supramolecules. The two corresponding melting points differ by 2 $^\circ\text{C}$, compared to a difference of 3 $^\circ\text{C}$

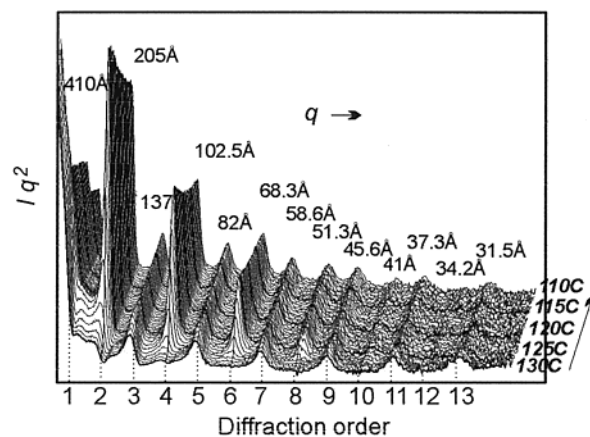


Figure 23. SAXS traces (Lorentz corrected intensities vs q) of n - $\text{C}_{191}\text{H}_{385}\text{COOH}$ recorded during cooling of an already partially crystallized sample at 0.3 $^\circ\text{C}/\text{min}$ from 132 to 112 $^\circ\text{C}$. Bragg spacings corresponding to the observed peak positions, recording temperatures and diffraction orders of the bilayer phase are marked (from ref 137 by permission of American Chemical Society).

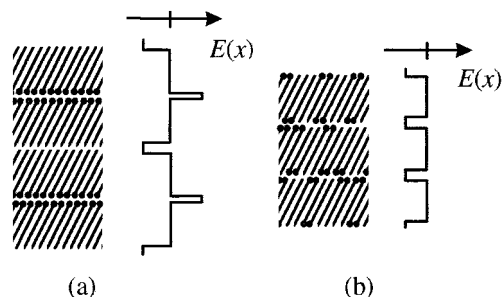


Figure 24. Schematic sketches of the double layer (a) and monolayer (b) structure of n - $\text{C}_{191}\text{H}_{385}\text{COOH}$. Circles represent carboxylic groups. Electron density profiles, $E(x)$, are shown schematically on the right (from ref 137 by permission of American Chemical Society).

between the melting points of extended and once-folded alkane $\text{C}_{390}\text{H}_{782}$ (see Table 3).

A comparative study has been performed on PEO fractions with molecular weights 3000 and 7100 having the following end-groups: hydroxy (HPEO), methoxy (MPEO), t -butoxy (TPEO), and phenoxy (PPEO).¹³⁹ Initial NIF long period l_{SAXS} obeyed the $c/(\Delta T)$ dependence, with the constant c decreasing in the series MPEO, HPEO, TPEO, PPEO. A similar descending series MPEO, TPEO, HPEO, PPEO was found in NMR diffusion coefficients. The differences are generally more pronounced for the 3000 fraction. The NIF \rightarrow IF transformation was also found to be retarded in the less mobile oligomers. Since the bulky end-groups tended to promote NIF rather than disfavor it, the results seem to support a model of NIF in which chain ends remain outside the crystal layer.

H. Monodisperse Block Copolymers

Although many block copolymers have a narrow molecular weight distribution, they will not be reviewed here as they present a broad subject of their own. Short uniform di-block chain compounds have been prepared and extensively studied in cases such

Table 3. Comparison of Melting Points of the Two Lamellar Forms of *n*-Alkanoic Acid C₁₉₁H₃₉₃COOH with Those of Integer Forms of Alkanes C₁₉₄H₃₉₀ and C₃₉₀H₇₈₂ (ref 138)

compd	form	T _m (°C)	form	T _m (°C)
C ₁₉₄ H ₃₉₀	extended	126.2 ± 0.3		
C ₁₉₁ H ₃₉₃ COOH	monolayer	130.0 ± 0.5	bilayer	131.9 ± 0.3
C ₃₉₀ H ₇₈₂	once-folded	129.0 ± 0.3	extended	132.0 ± 0.3

as alkyl-perfluoroalkyl diblocks^{140,141} and alkyl-oligo(oxyethylene) and similar nonionic surfactants. The current review is limited to long, truly monodisperse di-block and tri-block chain molecules. By doubling and tripling monodisperse ethylene glycol oligomers, such as pentadeca(ethylene glycol), Booth and co-workers prepared several series of C_nE_pC_n triblock copolymers, where E_p denotes *p*-mer of ethylene oxide and C_n a normal alkyl end-group C_nH_{2n+1}. For *p* ≤ 25, the E segment was crystalline (helical conformation) and extended, with the alkyl chain ends either amorphous (small *n*) or in a disordered crystalline state similar to the rotator phase (intermediate *n*). For *n* > 26 and at lower temperatures, the structure is dictated by the alkyls forming ordered crystalline layers. Here the E blocks are noncrystalline although in the predominantly planar zigzag conformation which better matches the cross-sectional area of the alkyl groups. From SAXS measurements it was concluded that for smaller *p* the E blocks are essentially extended, but for *p* = 15 and 25 they are once-folded. Only for *p* ≥ 45¹⁴² can both blocks be nearly completely crystalline. Extended, once-folded and noninteger forms are observed; the NIF converts to one of the IF forms at a higher temperature through melting and recrystallization.

Monodisperse diblock oligo(ethylene oxide) mono-*n*-alkyl ethers have also been prepared and studied.¹⁴³ Oligomers with hydroxy-ended E-blocks formed bilayer crystals (cf. Section II.G and Figure 22), and the methoxy-ended oligomers formed monolayer crystals. The helical oxyethylene blocks were perpendicular to the layer plane, while the alkyl blocks were generally tilted at 30° to the layer normal. Monodisperse triblock oligomers with a central methylene block and outer oxyethylene blocks were also studied subsequently¹⁴⁴ and both fully crystalline and partly crystalline structures were found, with chains in wholly trans-planar and mixed trans-planar/helical conformations.

An AFM study was carried out on thin crystalline films of a diblock and a triblock poly(oxyethylene)/poly(oxybutylene) (E/B) copolymer deposited on silicon.¹⁴⁵ At room-temperature E blocks are crystalline and B blocks are amorphous. The crystal thickness determined from AFM was compared to the bulk layer spacing determined by SAXS. It was shown that E₄₁B₂₂E₄₁ largely crystallizes in a monolayer form with unfolded E blocks at the substrate and folded B blocks at the polymer–air interface and with the E blocks tilted at an angle of ca. 40° to the substrate normal. Multiple layers with a common step height were observed for the diblock E₂₇B₆ crystallites, which were largely comprised of unfolded chains, also with E block tilted at an angle of ca. 40°.

I. Branched Oligomers

Cheng and co-workers have studied 2-, 3-, and 4-arm branched oligomer fractions where the PEO arms are connected via a benzene ring. Symmetrical two-arm PEO oligomers were prepared by coupling two chains of a PEO fraction with 1,4-benzene dicarbonyl dichloride.¹⁴⁶ In the material with the arm's molecular weight *M_n^a* = 2200, NIF crystals form initially, followed by apparent thinning during subsequent annealing. The lamellar spacing of NIF is longer than the extended chain length of one arm but shorter than that of the two-arm PEO. The long spacing of the final crystal, as well as its melting point, are similar to those of linear PEO with the length of a single arm. Similar but more complex behavior was observed in the two-arm PEO with *M_n^a* = 5500, where individual arms have the ability to fold.

Three two-arm PEOs with the same arm length (*M_n^a* = 2200) but coupled via different substitutions (1,2-, 1,3-, and 1,4-) of the benzene rings were further studied.^{147,148} The broad melting peak for samples crystallized at low supercoolings was regarded as composed of two overlapping components, and so was the first-order SAXS peak. It was postulated that the SAXS peak with shorter spacing corresponded to the extended chain conformation of the two-arm PEO, whereby one layer of benzene rings exists between two neighboring lamellae, while once-folded two-arm PEOs would have two phenylene layers lying between neighboring PEO lamellae and thus have a longer spacing. It was found further that by changing the coupling angle of the arms, i.e., changing from 1,4- (180°) to 1,2-substitution (60°), the extended conformation became increasingly difficult to achieve.

In the case of three- and four-arm PEOs, it was found that at low supercoolings the initial NIF lamellae undergo continuous thinning.¹⁴⁹ However, the final system has a 10–15% lower crystallinity (after weight correction for the coupling agent) compared to that of the equivalent linear PEO, suggesting that uncrystallized PEO arms exist between the crystalline layers. At high supercoolings, the long period remained constant. On subsequent heating the crystallinity decreases by about 10% (partial melting) and only increased slightly (by 1–2%) upon prolonged annealing. The underlying mechanism remains unclear.

Melt- or solution-crystallization of alkanes C₉₆H₁₉₃-CH(CH₃)C₉₄H₁₈₉ and C₉₆H₁₉₃CH(C₄H₉)C₉₄H₁₈, which contain a short branch in the center of an otherwise linear chain, always produced the once-folded (F2) conformation (see Figure 6f). In melt-crystallization, this is formed via a very short-lived NIF intermediary stage, see Figure 5b and Figure 6e. As described in Section II.C, the rapid NIF → F2 transition is

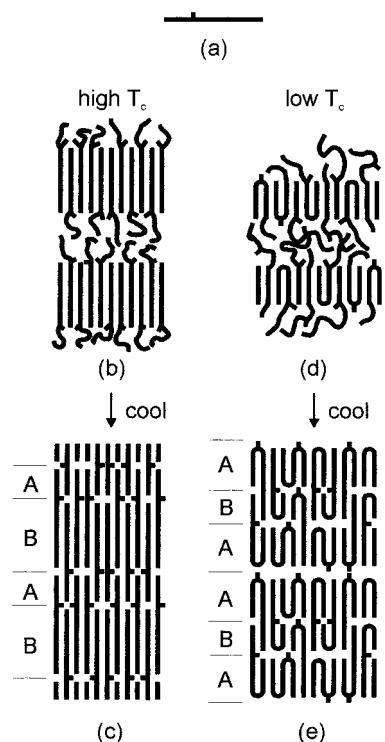


Figure 25. Schematic drawing of different lamellar structures observed in asymmetric methyl-branched alkane $C_{191}H_{383}CH(CH_3)C_{99}H_{199}$ (a); (b) semicrystalline form obtained at high T_c ; (c) double layer crystalline form obtained from panel b on cooling; (d) semicrystalline form obtained at low T_c ; (e) triple layer crystalline form obtained from panel d on cooling. Chain tilt is neglected in this and Figure 26, for simplicity (from ref 151).

believed to be due to the initial preference for “correct” chain attachment dictated by the exclusion of the branch to the lamellar surface.

The above butyl-branched alkane was studied by solid-state ^{13}C NMR, alongside its linear analogue $C_{198}H_{398}$, to establish the solid-state diffusion coefficient.¹⁵⁰ Both alkanes were in the once-folded form. The progressive saturation experiments have shown that the longitudinal relaxation of magnetization is consistent with a solid state chain diffusion process. Reptation and one-dimensional diffusion models were demonstrated to satisfactorily represent the data. The addition of the branch to the alkane chain was shown to result in a decrease in the diffusion coefficient, which ranged from $0.0918 \text{ nm}^2 \text{ s}^{-1}$ for the linear chain to $0.016 \text{ nm}^2 \text{ s}^{-1}$ for the branched chain. These diffusion coefficients are consistent with those of polyethylene.

Asymmetrically methyl-branched alkane $C_{191}H_{383}CH(CH_3)C_{99}H_{199}$ (Figure 25a), synthesized recently,¹⁰⁵ has been studied by real-time SAXS.¹⁵¹ The compound can be crystallized in two different semicrystalline forms, depending on crystallization temperature T_c . Electron density reconstruction has shown that in each case the structure consists of alternating crystalline and amorphous layers with respective thicknesses l_c and l_a ($l_c + l_a = l$). In the first form, obtainable only at high T_c , the longer arm of the alkane crystallizes as extended chain, while the shorter arm remains as a *cilium*, contributing to the

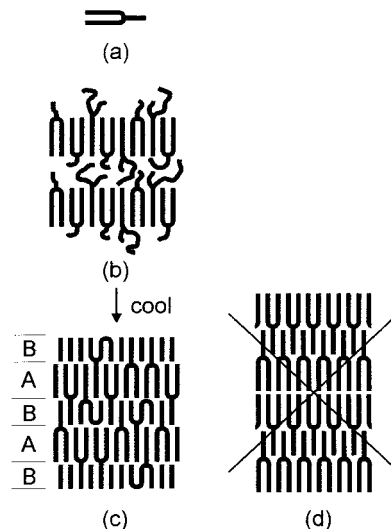


Figure 26. Schematic drawing of lamellar structures in Y-shaped alkane $C_{120}H_{241}CH(C_{61}H_{123})C_{119}H_{239}$ (a); (b) high-temperature semicrystalline form; (c) low temperature double layer crystalline form; (d) the hypothetical energy favored but kinetically unattainable structure (from ref 151).

amorphous layer (Figure 25b). At low T_c , another semicrystalline form is obtained. Here l_c is smaller and is determined by the length of the shorter arm. As shown in Figure 25d, the extended shorter arm and part of the longer arm may contribute to the crystalline layer, with the remainder of the long arm staying in the amorphous layer.

When either of the semicrystalline forms of the asymmetric alkane are cooled, they transform to a double-layer and a triple-layer crystalline structure, respectively. These 1-d superlattices are described as ABAB... and ABAABA... stacks of crystalline layers as depicted in Figure 25, panels c and e. Note that the structure in Figure 25e is related to the mixed integer “folded-extended” structure in some pure n -alkanes (Figure 7c) and in binary mixtures of long n -alkanes (Section II.J, Figure 30b).

Y-shaped alkane $C_{120}H_{241}CH(C_{61}H_{123})C_{119}H_{239}$, which has two long and one shorter arm (Figure 26a), has also been prepared¹⁰⁵ and investigated.¹⁵¹ A semicrystalline structure was found in the high-temperature region, with the crystalline layer thickness being determined by the length of the long arms. From the thickness of the amorphous layer l_a it was concluded that some molecules have both their long arms crystallized, but others have only one crystallized, the other two remaining in the amorphous layer (see Figure 26b). A double layer crystalline superstructure is formed in a transition on subsequent cooling, with one layer containing only long arms of the molecules and the other layer containing both extended short arms and folded long arms (see Figure 26c).

From the observations on branched PEO and alkanes more general conclusions can be drawn about the overcrowding problem at the crystalline–amorphous interface in polymers and about the mechanism of chain deposition during crystal growth. Thus, e.g., although for the Y-shaped alkane the energeti-

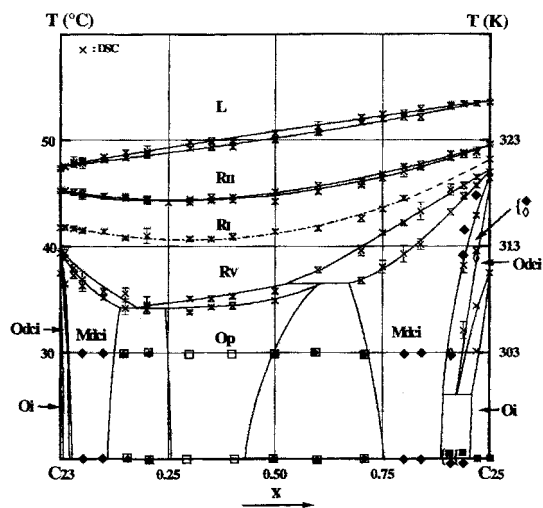


Figure 27. Binary phase diagram of the *n*-alkane system $C_{23}H_{48}$ – $C_{25}H_{52}$. Phases denoted with capital letters R, O, and M refer, respectively, to rotator, orthorhombic and monoclinic (from ref 157 by permission of Materials Research Society).

cally most stable state is that in Figure 26d, this state has proven to be kinetically unattainable. Further, by measuring the thickness of the amorphous layer l_a as a function of time and T_c one can obtain detailed experimental information on the number of chains crossing the crystal–amorphous boundary, giving valuable insight into the equilibrium and kinetic overcrowding effects, fold adjacency etc.

J. Binary Mixtures

A number of early studies have focused on phase diagrams of various binary *n*-alkane systems.^{152–154} General conditions for solid solution were set out by Kitaigorodskii¹⁵⁵ in terms of molecular size and symmetry. The maximum allowed difference in the number of C atoms has been stated empirically as¹⁵⁶

$$n_{\text{long}} = 1.224n_{\text{short}} - 0.411 \quad (4)$$

Binary phase diagrams of these shorter *n*-alkanes have turned out recently to be rather complex and subtle, even if the chain length difference is minimal and even in the case of two odd alkanes, where previously it was thought that miscibility is complete. Figure 27 illustrates this on the example of $C_{23}H_{48}$ – $C_{25}H_{52}$.¹⁵⁷ In the case of even alkanes, although the stable phases of the individual even component may be triclinic or monoclinic, the most prevalent crystal structures of the mixture is orthorhombic at low temperatures and rotator (usually pseudohexagonal) at higher temperatures.^{158–163} The orientationally disordered rotator phase allows improved miscibility close to the melting point, but with increasing chain length it is destabilized; it has not been seen to play a role in mixtures of long alkanes.

Because the length difference of the two miscible components is small, the disorder is considered mainly in terms of site occupancies close to the lamellar surface.^{159,163} Thus, alkane solid solutions provide good models of surface disorder, which has been studied by infrared and Raman spectro-

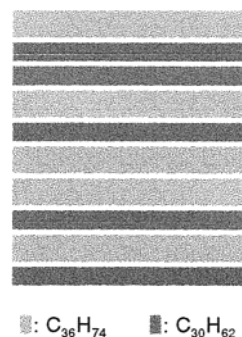


Figure 28. Proposed structural model of the $C_{30}H_{62}$ – $C_{36}H_{74}$ binary mixture. The $C_{30}H_{62}$ and $C_{36}H_{74}$ species are separated in individual layers, which stack randomly (after ref 163).

scopy.^{16,164,165} Alkane mixtures have also helped understand the nature of the rotator phase,^{21,160,166} as well as chain defects and molecular motion in general.¹⁶⁷ Phase change induced by mixing has been utilized in monitoring interdiffusion after crystals of different alkanes are put in mechanical contact.^{17,18,168}

Beside true solid solutions in which disparate molecules are intimately mixed, various modulated lamellar structures were observed in mixtures $C_{30}H_{62}$ + $C_{36}H_{74}$,¹⁶⁹ $C_{30}H_{62}$ + $C_{40}H_{82}$,¹⁷⁰ and $C_{28}H_{58}$ + $C_{36}H_{74}$.¹⁷¹ The structural models proposed were mostly based on random or nonrandom stacking of lamellae which were essentially composed of pure components¹⁶³ (Figure 28). Recent structural studies have been extended to multicomponent mixtures.¹⁷²

Crystallization theory and equilibrium thermodynamics of mixed alkanes have been discussed by Lauritzen, Passaglia, and DiMarzio¹⁷³ (LPD) and Asbach and Kilian.¹⁷⁴ In the LPD theory, the excess end-surface energy comes from exposed side surface due to nonuniformity in chain length. In contrast, Asbach et al. treat the enthalpy of mixing in more general terms. LPD theory has been applied to melting and the solid-state transition of binary mixtures of *n*-alkanes.¹⁷⁵

In contrast to the shorter alkanes, long *n*-alkanes were recently found to form solid solutions in a wide range of compositions, even if the chain lengths of the components differed by more than 100 C-atoms. Binary mixtures of long alkanes with the chain length ratio between 1.3 and 2 have been found to form predominantly two mixed phases, a high-temperature and a low-temperature one, separated by a reversible transition.¹⁷⁶ Figure 29 shows SAXS traces of the high-temperature form of four 1:1 w:w mixtures of $C_{162}H_{326}$ with a longer alkane of increasing length, including pure $C_{162}H_{326}$. The inset shows the corresponding best-fit electron density profiles perpendicular to the lamellae. The central high-density crystalline layer retains the same thickness l_c for all mixtures; however, the thickness of the low-density amorphous layer l_a increases in proportion with the surplus length of the longer alkane. Accordingly, the structural model in Figure 30a was proposed: while the shorter alkane is fully crystalline and confined to the crystal layer, the longer alkane chains traverse the crystal layer and the surplus length, the *cilia*,

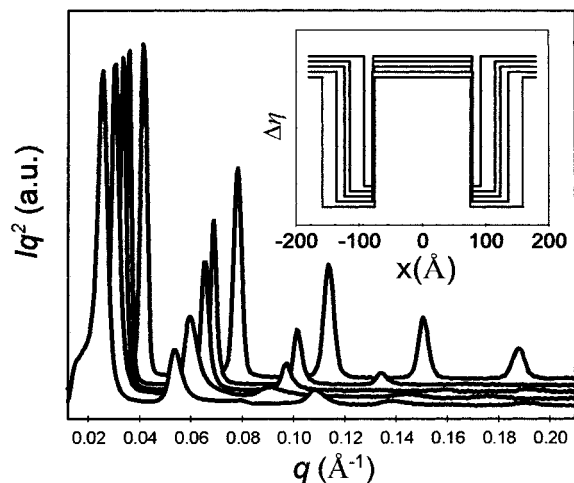


Figure 29. Small-angle diffractograms of $C_{162}H_{326}$ and of the high-temperature phase of 1:1 w:w binary mixtures of $C_{162}H_{326}$ with, from top to bottom, $C_{194}H_{390}$, $C_{210}H_{422}$, $C_{246}H_{494}$, and $C_{258}H_{518}$. The inset shows the corresponding best-fitting electron density model profiles (from ref 176 with permission of the American Physical Society).

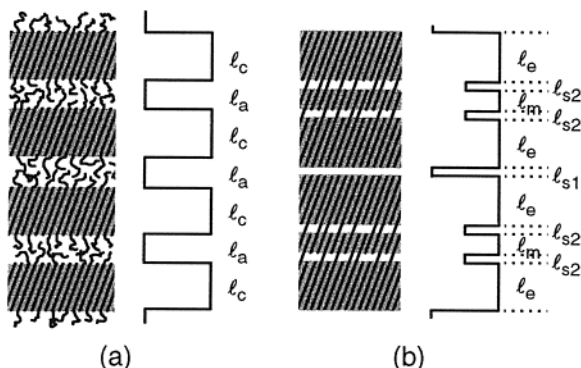


Figure 30. Schematic structures of (a) the high-temperature semicrystalline phase, and (b) the low-temperature triple-layer superlattice in binary long alkanes. Model electron density profiles are shown on the right, with density increasing from left to right (from ref 176 with permission of the American Physical Society).

form the amorphous layer. This “semicrystalline form” (SCF) is related to the NIF form in pure alkanes (Section II.C), where the role of the shorter alkane is taken by folded chains. In contrast to the NIF form, the SCF in binary alkanes is the thermodynamically stable form within a given range of temperatures and compositions.^{176,177} SCF is also related to the high-temperature forms of branched long alkanes (Figure 25b,d and Figure 26b), some of which are also stable.

Below the phase transition temperature, the SAXS pattern of the binary mixtures becomes complex, but curve resolution and Fourier synthesis revealed a superlattice structure based on a triple-layer repeat unit as shown in Figure 30b.¹⁷⁶ The two outer layers l_e contain extended chains of the shorter alkane (e.g., $C_{162}H_{326}$) as well as the major portion of the longer chain molecules (e.g., $C_{246}H_{494}$). The middle layer l_m contains only the surplus length of the longer molecules protruding from the two end-layers. All three layers are crystalline, although there is evidence from WAXS, calorimetry and Raman LAM spectroscopy

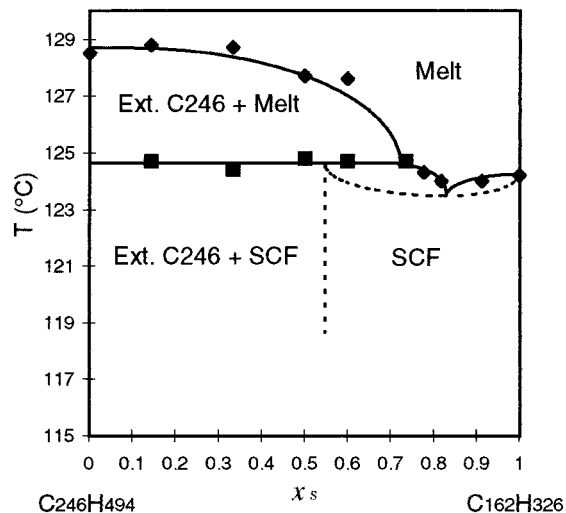


Figure 31. Equilibrium phase diagram of the $C_{162}H_{326}$ – $C_{246}H_{494}$ binary system. x_s = molar fraction of $C_{162}H_{326}$, Ext. C246 = extended-chain $C_{246}H_{494}$, SCF = semicrystalline form (from ref 177a with permission of the American Chemical Society).

that crystal perfection of the middle layer is poor. The transition between the SCF and the triple-layer superlattice is thought to occur through a cooperative process with pairs of SCF layers acting in tandem.

The equilibrium phase diagram of the $C_{162}H_{326}$ – $C_{246}H_{494}$ binary system (high-temperature range) is shown in Figure 31. The most important feature is the phase boundary of the semicrystalline phase. At temperatures below the triple point the single phase SCF was found to be stable in the range $0.56 \pm 0.04 < x_s < 1$, where x_s is the molar fraction of the shorter alkane $C_{162}H_{326}$. The reason that a SCF phase with $x_s < 0.56$ is unstable is believed to be due to steric overcrowding at the crystalline–amorphous interface. In the case of polyethylene it has been recognized that the cross-section area required by an amorphous chain is at least twice that required by a straight crystalline chain.^{178–180} In polymers, the overcrowding problem is resolved partly by chain tilt (see Section II.E), but for the greater part by adjacently re-entrant chain-folding. In the case of a mixed alkanes with high x_s , the overcrowding problem is resolved by the shorter chains ending at the crystal surface. However, for $x_s < 0.56$ the problem becomes insoluble and the excess longer component phase separates. Since the chains in SCF are tilted by 35° , it follows that the effective cross-section area of a chain crossing the crystalline–amorphous interface increases by a factor of $(0.44 \cos 35^\circ)^{-1} = 2.8$.

Studying shorter n -alkanes, Bonsor and Bloor¹⁷⁵ have suggested the possibility of two short chains substituting for one longer chain in a solid solution of molecules with a length ratio 1:2. Their experimental results on the binary system $C_{19}H_{40}$ – $C_{44}H_{90}$ were inconclusive. In contrast, in binary long n -alkanes such as $C_{122}H_{246}$ – $C_{246}H_{494}$, crystalline solid solutions were indeed shown to form readily; however, in this case the long chains ($C_{246}H_{494}$) are either folded or extended, while the short chains are extended.¹⁸¹ The resulting structure is a triple-layer superlattice, similar to that in Figure 7c, and the

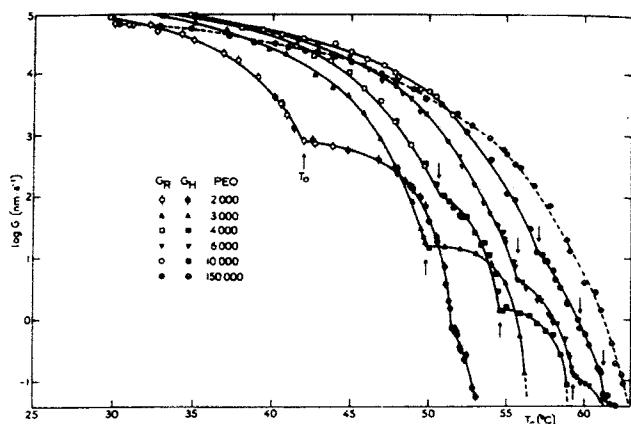


Figure 32. Temperature dependence of growth rate G_H of $\{010\}$ faces of single crystals and G_R of spherulites for five low molecular weight fractions and a polymer of PEO (from ref 28 by permission of John Wiley & Sons.).

thickness of the basic layer unit is determined by the length of the shorter $C_{122}H_{246}$ chain.⁶¹

III. Crystallization Process and Morphology

A. Stepwise Growth Rate vs Temperature Gradient

Studies on PEO fractions in the molecular weight range between 1500 and 12 000 have shown²⁸ that the slope of the increasing crystal growth rate with supercooling $dG/d(\Delta T)$ increases sharply at a series of specific crystallization temperatures T_c^m ($m = 1, 2, 3, \dots$). These mark the transitions between the growth of crystals with $m-1$ and m folds per chain. Figure 32 shows the temperature dependence of the growth rate from the melt normal to the $\{010\}$ lateral face for five low molecular weight fractions and a polymer (note the log rate scale). The breaks in the slope at T_c^m are particularly pronounced in low molecular weight fractions and are completely lost in the polymer. The existence of such sharp increases in $dG/d(\Delta T)$ is, at least qualitatively, entirely predictable by the secondary nucleation theory once quantization of lamellar thickness is accepted.¹⁸ The supercoolings at which growth transitions occur, relative to the melting point of extended chains, are given by

$$\Delta T_c^m = \frac{2\sigma_{e(\infty)}T_m}{\Delta h_f} \left(\frac{m}{m+1} \right) \left[\left(\frac{L}{m+1} \right) - \delta \right] \quad (5)$$

Here $\sigma_{e(\infty)}$ is the fold-surface free energy for $L = \infty$, and Δh_f is heat of fusion. δ is a small constant, reflecting the fact that some finite supercooling is required for crystal growth (see Section III.E). Equation 5 can be used for the determination of accurate $\sigma_{e(\infty)}$ for the parent polymer.

According to the secondary nucleation theory, polymer crystals grow by deposition of layers of stems on the side surface of the lamella¹⁸³ (see Figure 33). Each new layer needs to be nucleated ("secondary" or surface nucleation), after which it spreads comparatively rapidly. The main barrier to secondary nucleation is the excess side surface free energy $2b\sigma$

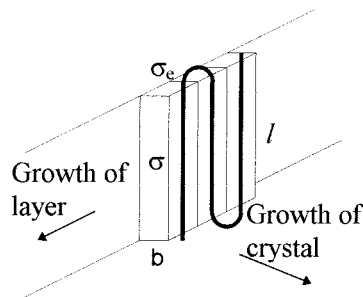


Figure 33. Chain deposition on the side surface of a polymer crystal. σ and σ_e are side-surface and end (fold-) surface free energies, b is the width of the chain (after ref 183).

for the creation of the two new surfaces either side of the single-stem nucleus; here b is the chain width and σ the side surface free energy. For polymer crystals of fixed fold length l , the slope $dG/d(\Delta T)$ should be constant within the limited temperature interval that is accessible for studying.¹⁸⁴ Indeed, when plotted on a linear scale, the growth rates G vs ΔT dependence in Figure 32 does not deviate much from linearity for a given m .¹⁸⁵ However, linear G vs ΔT is also consistent with the alternative polymer crystallization theory, the so-called "roughness-pinning theory" of Sadler.^{185,186} According to this theory, the difference between nucleation and growth of molecular layers on the growth face is negligible and the growth surface is rough rather than smooth (see Section III.E).

On closer scrutiny the crystal growth data for PEO fractions deviated somewhat from those expected from secondary nucleation theory; there were departures from linearity of G vs ΔT near the T_c^m transition temperatures,¹⁸⁵⁻¹⁸⁸ and the value of σ derived from the kinetics was unrealistically low.¹⁸⁷

B. Crystallization Rate Minima and Negative Order Kinetics

Crystallization rate experiments on monodisperse n -alkanes have shown a rather different picture. Not only is there a sharp increase in $dG/d(\Delta T)$ at the transition between extended and once-folded (or NIF) crystallization mode ($T_c^{m=1}$) but the $dG/d(\Delta T)$ gradient actually becomes *negative* as $T_c^{m=1}$ is approached from above.¹⁸ This was found to occur both in crystallization from melt¹⁸⁹ and from solution,¹⁹⁰ and it applies both to crystal growth and primary nucleation.¹⁹¹ Figure 34 shows the way G passes through a maximum and reaches a sharp minimum at the transition from extended to once-folded chain crystal growth of $C_{198}H_{398}$ from solution for two different concentrations.¹⁹² The rate minimum at $T_c^{m=1}$ has been observed in a number of alkanes from $C_{162}H_{326}$ to $C_{294}H_{590}$.¹⁹³⁻¹⁹⁶ In alkane $C_{294}H_{590}$, where crystallization rate from solution is sufficiently low for $T_c^{m=2}$ to be accessible, a crystallization rate minimum has been observed between the once-folded and twice-folded growth intervals.¹⁹⁷ A weak minimum at $T_c^{m=1}$ has also been reported in melt-crystallization of a methyl-terminated PEO fraction.¹⁹⁸

The negative $dG/d(\Delta T)$ observed in alkanes has been attributed to an effect termed "self-poisoning".¹⁸⁹

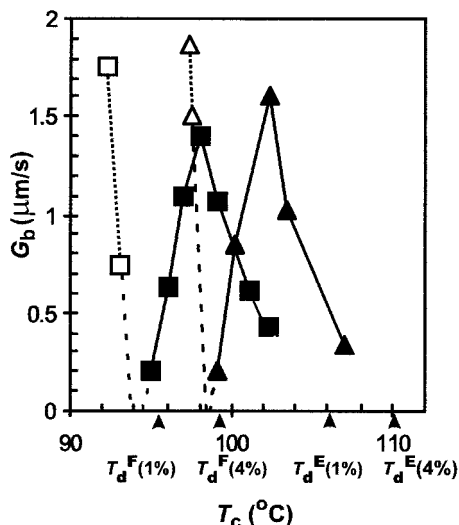


Figure 34. Initial crystal growth rate (G_b along [010]) vs crystallization temperature from 1.1 wt % (■, □) and 4.2 wt % solutions (▲, △) of $C_{198}H_{398}$ in 1-phenyldecane. (■, ▲) extended chain, (□, △) once-folded chain crystals. T_d^E and T_d^F are the dissolution temperatures of extended-chain and once-folded-chain crystals. The retardation in growth around T_d^F is caused by “self-poisoning” (from ref 192 by permission of American Physical Society).

This proposed mechanism recognizes the fact, highlighted by the roughness-pinning crystallization theory of Sadler, that chains wrongly attached to the crystal surface may hinder further growth. This blocking, or “pinning”, may be overlooked in polymers, but in monodisperse oligomers, it becomes very pronounced as, e.g., the folded-chain melting point T_m^F is approached from above. Although only extended-chain depositions are stable, close to T_m^F , the lifetime of folded-chain depositions becomes significant. As extended chains cannot grow on a folded-chain substrate,²⁸ growth is temporarily blocked until the folded-chain overgrowth detaches. At T_m^F itself the detachment rate of folded chains drops to the level of the attachment rate and the entire surface is blocked for extended chains.

The growth rate minima cannot be explained by the secondary nucleation theory in its present form because the competing attachments to the growth face are ignored and the deposition of a whole stem is treated as a single event.¹⁹⁹ However, the minimum in G is well reproduced, at least qualitatively, with even the simplest departure from the classical approach, i.e., by splitting the stem, or the alkane chain, into two segments and allowing the second segment the choice of aligning coaxially with the first segment (extended chain) or alongside it (folded chain) (see Figure 35).²⁰⁰ The forbidden step is attachment of an extended chain onto a folded chain. A Monte Carlo simulation study, where these same selection rules were applied, has also reproduced the kinetics of the self-poisoning minimum and has provided some additional insight into the crystal shape.²⁰⁰

Another manifestation of the self-poisoning effect is the anomalous negative order kinetics of crystallization from solution. In long alkanes, there is a supersaturation range in which crystal growth rate

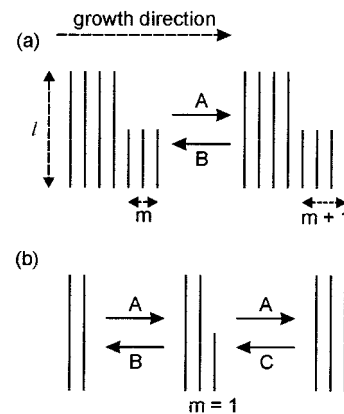


Figure 35. The model of elementary steps as used in the rate equation and Monte Carlo simulation treatments that reproduced the self-poisoning minimum. A cross-section (row of stems) normal to the growth face is shown. There are three elementary steps differing in their barrier and driving force: attachment (rate A) and detachment (rate B) of segments equal to half the chain length, and partial detachment of an extended chain (rate C). The key self-poisoning condition is that attachment of the second half of an extended chain is allowed only if $m = 1$, i.e., an extended chain cannot deposit onto a folded chain (from ref 200 by permission of the American Institute of Physics).

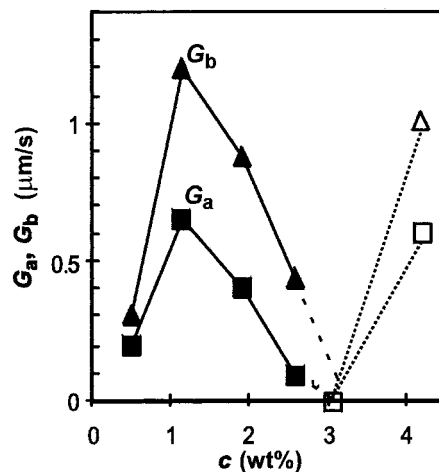


Figure 36. Initial crystal growth rate G_a (along [100]) and G_b (along [010]) of $C_{198}H_{398}$ vs solution concentration at 98.0 °C. (■, ▲) Extended chain, (□, △) once-folded chain crystals. Note the negative dG/dc gradient for $1\% < c < 3\%$ (from ref 192 by permission of American Physical Society).

actually *decreases* with increasing concentration c .¹⁹² For n - $C_{198}H_{398}$, this range is from 1 to 3% (see Figure 36). The two-segment-stem rate equation model of ref 200 has been adapted to include solution concentration, and again, both the G vs c and G vs T minima were reproduced well (see Figure 37, panels a and b). The calculated *temperature* dependence of G (Figure 37b) should be compared with the experimental data in Figure 34. The unusual retardation in crystal growth with increasing *concentration* in Figure 37a should be compared with Figure 36. This effect can be explained as follows. For $c < 3\%$, the attachment rate A is lower than the folded-chain detachment rate B^F , so only extended chains can grow. However, as $c = 3\%$ is approached, A becomes comparable to B^F and an increasing fraction of the growth face equal to A/B^F is covered by folded chains

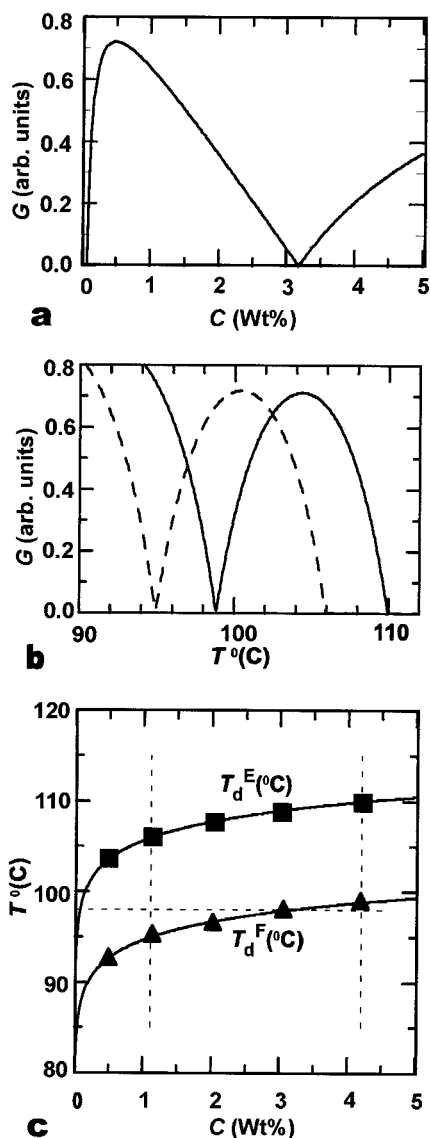


Figure 37. (a) Crystal growth rate G of n -C₁₉₈H₃₉₈ calculated as a function of concentration at $T_c = 98.0$ °C, cf. Figure 36. (b) G calculated as a function of T_c for $c = 1.1\%$ (dashed) and $c = 4.2\%$ (full), cf. Figure 34 (c). Binary phase diagram C₁₉₈H₃₉₈ - phenyldecane. Equilibrium liquidus curve $T_d^E(c)$ for extended chain crystals and non-equilibrium curve $T_d^F(c)$ for once-folded chain crystals were calculated, matched to the experimental dissolution temperatures (■, ▲) using three fitting parameters. Experimental $T_d^E(c)$ and $T_d^F(c)$ values were determined in situ at near zero heating rate (from ref 192 by permission of American Physical Society).

at any time. Hence the extended-chain crystal growth rate is

$$G^E = (1 - A/B^F)(A - B^E) \quad (6)$$

and as $c \rightarrow 3\%$ and $A \rightarrow B^F$, so $G^E \rightarrow 0$.

Figure 37c shows the alkane-solvent phase diagram calculated by equating $A = B^E$ (top curve: equilibrium liquidus) and $A = B^F$ (bottom curve: metastable liquidus). Imagining that crystal growth rate G is plotted on the z -axis, and bearing in mind that on either of the liquidus lines G is zero, the c and T dependencies of G in Figure 37a and b can be

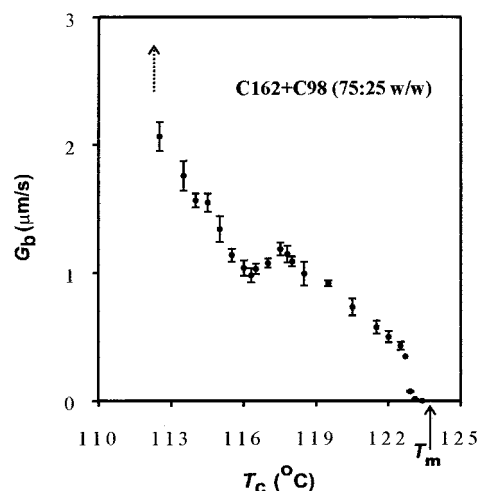


Figure 38. Crystal growth rate G_b vs temperature for a 75:25 w:w mixture of C₁₆₂H₃₂₆ and C₉₈H₁₉₈. The “poisoning” minimum at the melting point of C₉₈H₁₉₈ (116 °C) is seen. The steep increase in G below 112.5 °C (out of scale) is due to the transition to once-folded C₁₆₂H₃₂₆ growth (from ref 203).

visualized, respectively, as horizontal and vertical cuts through the phase diagram.

If the initial solution concentration c is higher than that corresponding to the maximum in G , then G will initially increase during the crystal growth as c decreases. This auto-accelerated crystallization gives rise to a further phenomenon, described as “dilution wave”.¹⁹² Thus, e.g., crystallization from an initially 4.2% phenyldecane solution of C₁₉₈H₃₉₈ at $T_c = 97.4$ °C results in folded-chain crystals which soon cease to grow as the metastable equilibrium is reached between folded-chain crystals and the pseudo-saturated solution (lower liquidus in Figure 37c). As both nucleation and growth of extended-chain crystals are highly suppressed under these conditions, no visible change occurs for some considerable time, after which rather suddenly the folded-chain crystals are replaced by needle-shaped extended-chain crystals. The transformation sweeps through the suspension. As the first extended-chain crystal forms successfully, it depletes the surrounding solution and thus triggers the growth of other extended-chain crystals in the vicinity. A “dilution wave” is thus generated easing the inhibitory effect of high concentration on extended-chain growth. The reaction diffusion equation describing the dilution wave has been found²⁰¹ to coincide with that used in genetics to describe the spread of an advantageous gene.²⁰² The wave spreading rate is determined by the polymer diffusion constant and the crystal growth rate G^E .

Recently, a new type of growth rate minimum has been induced above $T_c^{m=1}$ in melt-crystallization of several n -alkanes by the admixture of a shorter alkane with the melting point between those of the extended and once-folded-chain crystals of the host.²⁰³ Figure 38 illustrates this on the example of a 75:25 w:w mixture of C₁₆₂H₃₂₆ and C₉₈H₁₉₈. A relatively small but reproducible minimum is observed at 116 °C, in the middle of the extended-chain growth range of C₁₆₂H₃₂₆; this temperature coincides with the melting point of C₉₈H₁₉₈. Here the retardation and

the negative $dG/d(\Delta T)$ slope above 116 °C are not due to “self-poisoning” but rather to “poisoning” by the $C_{98}H_{198}$ chain attachments which are nearly stable and are thus blocking the growth face of the host crystals. Below the temperature of the minimum there is no drastic increase in $dG/d(\Delta T)$ since (a) $C_{98}H_{198}$ cannot grow rapidly as a minority component and (b) the growth is retarded by folded-chain $C_{162}H_{326}$ depositions due to the vicinity of $T_c^{m=1}$. Indeed, below $T_c^{m=1} = 112.5$ °C, there is a very steep increase in G as chain-folded crystallization of $C_{162}H_{326}$ takes over, incorporating the guest $C_{98}H_{198}$ chains in a semicrystalline NIF-type structure described in Section II.C.

Lower crystal growth rates in alkane $C_{162}H_{326}$ were also reported when a fraction of a shorter ($C_{122}H_{246}$) or a longer alkane ($C_{246}H_{494}$) was added.²⁰⁴ The addition of $C_{122}H_{246}$ had a somewhat larger retarding effect.

C. Crystallization and Morphology

The shapes of melt-grown single crystals of narrow PEO fractions have been studied in great detail by Kovacs and co-workers.^{28,29,64} Particular attention was paid to the narrow temperature range of the extended to folded-chain growth transition. Careful investigation revealed that there are in fact three close transition temperatures, one for each of the three $\{hk0\}$ growth face types. These differences, combined with the thickening process, resulted in “pathological” crystals, to be discussed briefly in the next section. A more general observation is that more or less faceted crystals grow at most temperatures, except just above the transition temperature range $T_c^{m=1}$, where crystals are rounded and sometimes indeed circular. This has been confirmed by subsequent studies, as illustrated in Figure 39.¹⁹⁸

The discovery of rounded polymer crystal edges^{99,205} has motivated Sadler to propose the rough-surface theory of crystal growth.¹⁸⁶ However, it was shown subsequently^{206–208} that the curvature of $\{100\}$ faces in polyethylene can be explained quantitatively by applying Frank’s model of initiation and movement of steps.²⁰⁹ Curvature occurs when the average step propagation distance is no larger than several stem widths, which places this type of crystal growth at the borderline between nucleated and rough-surface type. Thus, the increase in curvature of PEO crystal faces immediately above $T_c^{m=1}$ (Figure 39) means a reduction in the ratio v/i , where i is the initiation rate and v the propagation rate of new layers of stems. A connection has been made between the rounding of PEO crystals and a conspicuous downward deviation from linearity of measured G vs ΔT just above $T_c^{m=1}$.¹⁸⁵ In the past, the effect had been attributed to impurities,¹⁸⁸ but, subsequently, it was suggested to have been caused by self-poisoning.²¹⁰ Since $G = b \sqrt{2iv}$, the retardation in G combined with the reduction in v/i was taken to mean that the propagation rate of new surface layers v is more obstructed than their nucleation i . The blocking of niches retarding v and leading to a rounded face is schematically drawn in Figure 40.

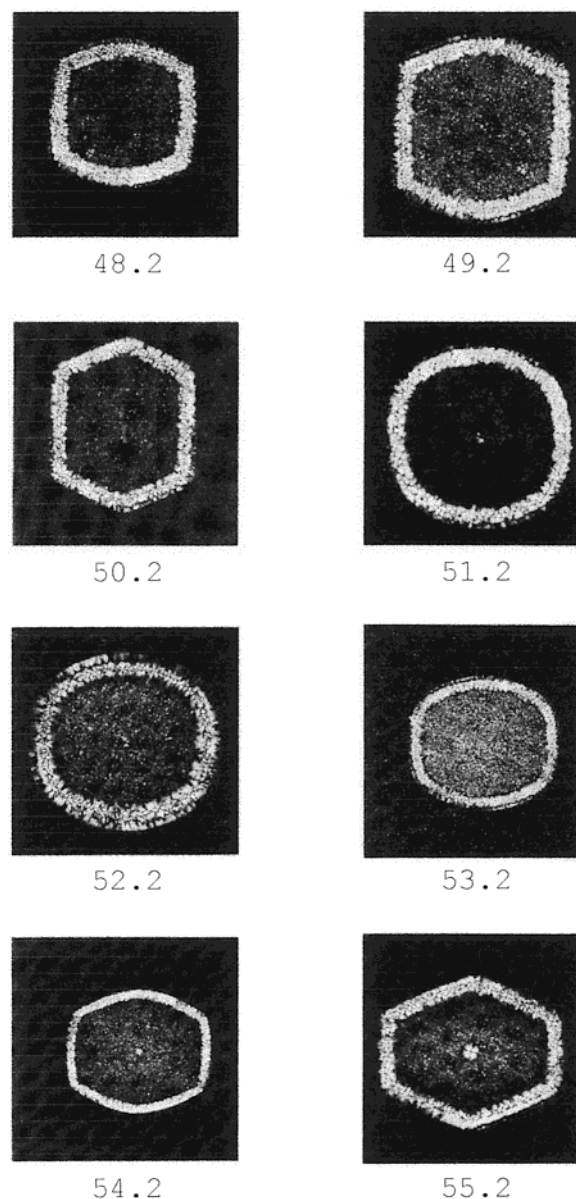


Figure 39. Optical micrographs of PEO single crystals (fraction $M_n = 3000$) grown from the melt as a function of crystallization temperature (°C). The extended–folded chain growth transition $T_c^{m=1}$ is between 51.2 and 50.2 °C (adapted from ref 198).

Whereas melt-grown single crystals of PEO fractions become rounded near the extended- to folded-chain growth transition, crystals of long alkanes show a whole range of morphologies within the temperature interval of extended-chain growth, both from melt and from solution.^{191,192,211} Figure 41 shows how the crystal habit in solution-grown $C_{198}H_{398}$ changes with decreasing T_c from perfect rhombic lozenges with $\{110\}$ lateral facets (a), through nearly hexagonal “truncated lozenges” ($\{110\}$ and $\{100\}$ faces) (b), through leaf-shaped (“lenticular”) crystals with curved $\{100\}$ faces (c, d), finally ending with needlelike crystals bounded by practically straight $\{100\}$ faces just above the growth rate minimum (e). On lowering T_c , further chain-folded crystallization takes over and the habit reverts to that of truncated lozenges (f). At still lower T_c (not shown), the shape changes to

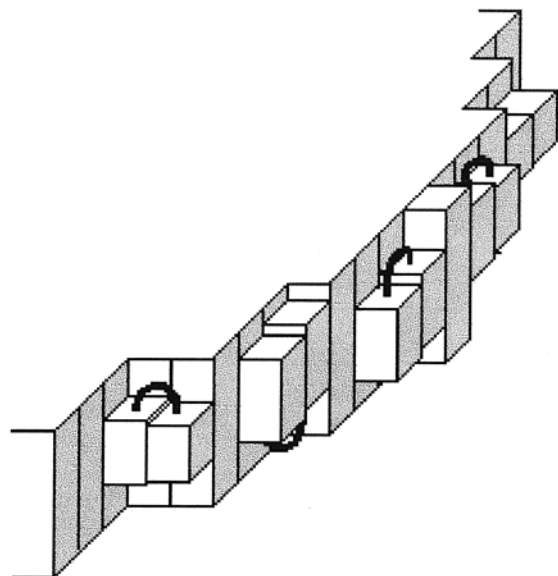


Figure 40. Schematic representation of a growth face of an extended-chain crystal with step propagation hindered by transient folded-chain depositions (from ref 210, by permission of Kluwer Academic Publishers).

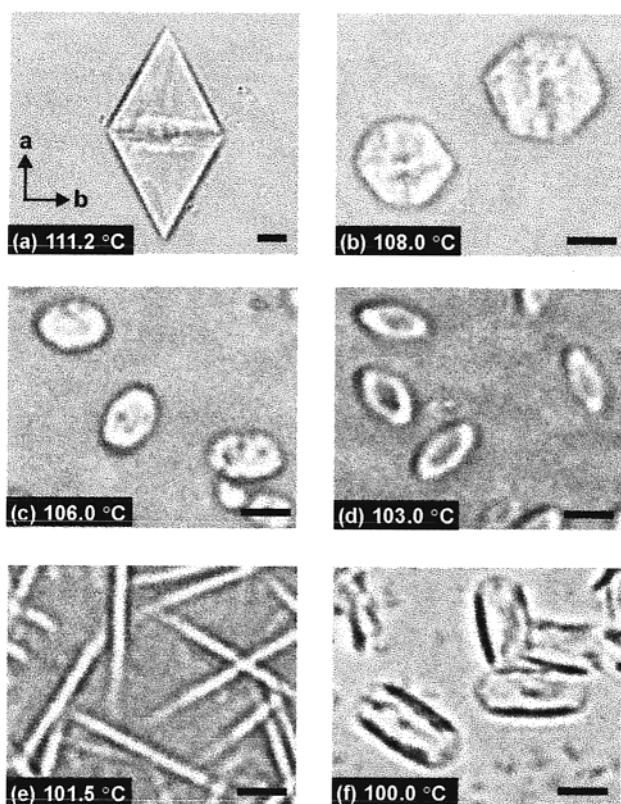


Figure 41. Series of in situ optical micrographs (interference contrast) of $n\text{-C}_{198}\text{H}_{398}$ lamellar single crystals grown from octacosane (initially 2%) at the temperatures indicated. (a–e) extended chain, (f) once-folded chain. Bar length represents 10 μm (from ref 214).

lenticular and the cycle is repeated. The remarkable feature is that the T_c dependence of crystal habit within one such cycle is the exact reversal of that in solution-crystallized polyethylene. In polyethylene rhombic {110}, lozenges grow at low T_c and with increasing temperature the habit changing gradually

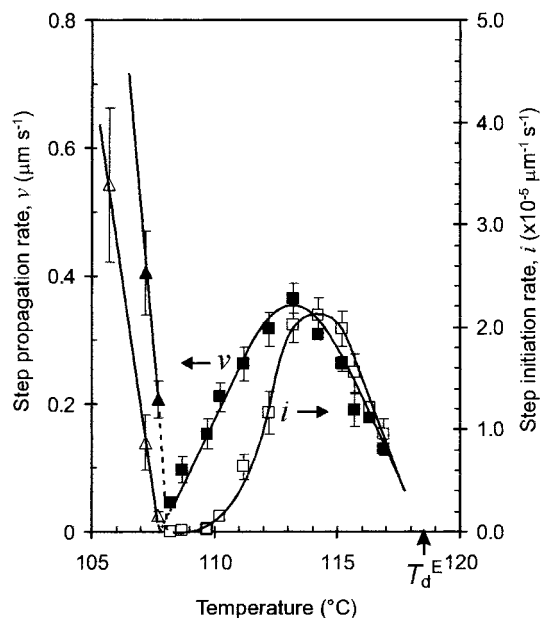


Figure 42. Initiation rate i (empty symbols) and propagation rate v (full symbols) of new steps on the {100} growth face of $n\text{-C}_{246}\text{H}_{494}$ crystals in 5% octacosane solution as a function of crystallization temperature. (■, □) Extended chain, (▲, △) once-folded chain (from ref 214).

toward elongated lenticular crystals which grow at the highest T_c from either solution or from melt.^{207,212}

The morphological changes described and exemplified in Figure 41 are determined, essentially, by the temperature dependence of only two parameters: (a) the ratio of growth rates normal to {110} and {100} faces, G_{110}/G_{100} and (b) the ratio v/i for {100} growth. Thus rhombic lozenges bounded by {110} lateral faces will be seen for any $G_{110}/G_{100} \leq \cos(\varphi/2)$, where $\varphi/2 = \tan^{-1}(a/b)$ and a, b are unit cell parameters. As T_c is reduced and the growth minimum is approached, G_{110}/G_{100} increases beyond the value of $\cos(\varphi/2)$, and the lozenges become truncated by {100} faces. The temperature dependencies of G_{100} and G_{110} are different, and for all alkanes, the growth normal to {100} faces is more retarded by self-poisoning than the growth normal to {110} faces. This applies both to solution²¹¹ and to melt crystallization.²⁰³ On the other hand, the curvature of the {100} faces is determined by the ratio of step propagation and step initiation rates v/i on these faces.

The profiles of the curved “{100}” faces in solution- and melt-crystallized alkanes were fitted to those calculated according to Mansfield,²⁰⁶ taking account of the centered rectangular lattice representative of polyethylene and alkanes.²¹³ As an example, i and v values thus obtained are plotted against T_c for $\text{C}_{246}\text{H}_{494}$ (5% in octacosane) in Figure 42.²¹⁴ While both the nucleation rate and propagation rate of steps on {100} faces pass through a maximum and a minimum as a function of T_c , and then increase steeply in the chain-folded temperature region, there is a significant difference in the shape of the two graphs near the growth rate minimum. In this and other examples of solution crystallization, initiation (i) is considerably more suppressed by self-poisoning than propagation (v), and the slope $d i/d(\Delta T)$ turns

negative further away from the minimum, (i.e., at a higher temperature) than the corresponding slope $dv/d(\Delta T)$. At the minimum, the $\{100\}$ faces are straight (see needlelike crystals in Figure 41e), this time not because layer completion is uninhibited, but rather because i is extremely low.

Comparing the morphological changes in melt-grown crystals of PEO fractions (see above, Figure 39 and Figure 40) and solution-grown crystals of long alkanes, we find that v is more affected by self-poisoning in PEO while i is more affected in the alkanes. Furthermore, the case of melt-crystallization of n -alkanes is closer to that of solution-crystallized alkanes.²⁰³ The difference between PEO and alkanes is not yet understood.

The cause of the changes in crystal habit with changing T_c in polyethylene, or in any other polymer for that matter, is unknown. These changes have a profound effect on morphology of industrial polymers. Thus, in melt-solidified polyethylene crystals grow along the crystallographic b -axis with lenticular morphology similar to that formed from polyethylene solutions at the highest T_c ^{99,100} or from long alkanes at the lowest T_c within the extended-chain regime (Figure 41, panels d and e). Hoffman and Miller²¹⁵ proposed that the retardation in v , leading to curved crystal edges, comes from lattice strain imposed by the bulky chain folds in the depositing chains; this results in strain surface energy σ_s which acts by slowing down the substrate completion process. To be consistent with the observed morphology in polyethylene, σ_s would have to be higher on $\{100\}$ faces than on $\{110\}$ faces. However, it is difficult to see how this argument would apply to crystallization of extended-chain n -alkanes with no chain folds.

Since the morphological trend with increasing T_c in polyethylene is the exact opposite of that observed in alkanes, and since the latter seems to be clearly associated with self-poisoning, it is tempting to interpret the changes in polyethylene as being due to an increasing effect of self-poisoning with increasing T_c . Self-poisoning in polydisperse polymers, if present, would be difficult to detect from crystallization kinetics, since lamellar thickness l changes continuously with T_c , and thus, no rate minima can be expected. However, self-poisoning is envisaged to affect crystal growth in the following manner. At any T_c , there is a minimum fold length l_{\min} below which attachments are more likely to melt than be built into the crystal. However, chain segments which are only slightly shorter than l_{\min} will have a reasonably long lifetime as well as a higher attachment rate because of the lower barrier $E^* = 2bl\sigma$. This would cause self-poisoning at any T_c . A snapshot of a cut normal to the surface of a growing crystal might thus look as in Figure 43. This situation corresponds to the "kinetic roughness" in the roughness-pinning model of Sadler¹⁸⁶ (see Section III.E). The reason for self-poisoning in polyethylene being more pronounced at higher T_c , as suggested by morphology, is one of a number of open questions.

While extended-chain crystals of $C_{162}H_{326}$ and $C_{198}H_{398}$ grown from octacosane at the smallest supercooling are faceted rhombic lozenges (see Figure

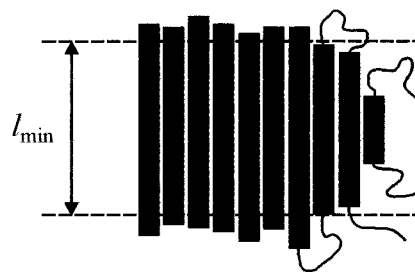


Figure 43. A possible instantaneous configuration of a row of stems perpendicular to the crystal surface schematically illustrating self-poisoning in a polydisperse polymer. The same picture could apply to a layer of stems depositing onto the crystal surface and parallel to it; in that case it would illustrate the retarding effect on layer spreading rate v (see also Section III.E).

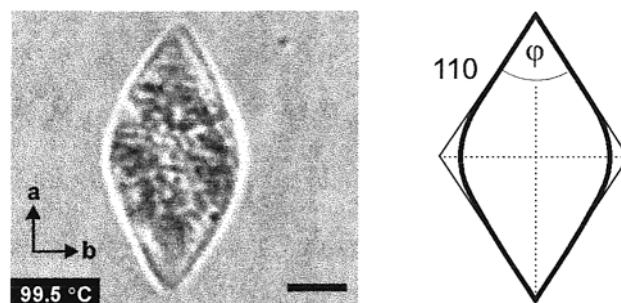


Figure 44. (Left) An "a-axis lenticular" crystals of $C_{162}H_{326}$ in 1-phenyldecane grown from an initially 1.0% solution at 99.5 °C. Interference optical micrograph. Bar length 10 μm . (Right) Schematic outline of the crystal, indicating the four $\{110\}$ sectors (from ref 211 with permission of the American Chemical Society).

41a), those grown under similar conditions from 1-phenyldecane have an unusual habit shown in Figure 44.²¹¹ This habit has not been seen in polyethylene and it has been termed "a-axis lenticular" because, unlike the more common lenticular (lens-like) polyethylene crystals, its long axis is parallel to the crystal a -axis. In fact, the habit can be best described as being bounded by curved $\{110\}$ faces. The interesting feature is the asymmetry of the curvature; while the faces are curved at the obtuse apex, they are straight at the acute apex. This has been attributed to the propagation rates of steps on the $\{110\}$ face being different in the two directions; the rate v_s , directed toward the acute apex, is higher than the rate v_b directed toward the obtuse apex. Similar asymmetry may be expected in other polymers where the growth face lacks a bisecting mirror plane normal to the lamella.

Crystallization of alkanes from dilute solutions (typically 0.01% or less) in good solvents such as toluene results invariably in faceted crystals, as shown already very early on $C_{94}H_{190}$ ²¹⁶ and subsequently on longer alkanes.⁶⁸

Morphology of long alkanes is also being studied in order to evaluate the role of cilia in lamellar splay, a key factor in the formation of polymer spherulites.^{204,217} The hypothesis is that cilia exert an entropic repulsive force when crystalline lamellae approach each other closely. Earlier results seemed to have indicated that in long alkanes spherulites are

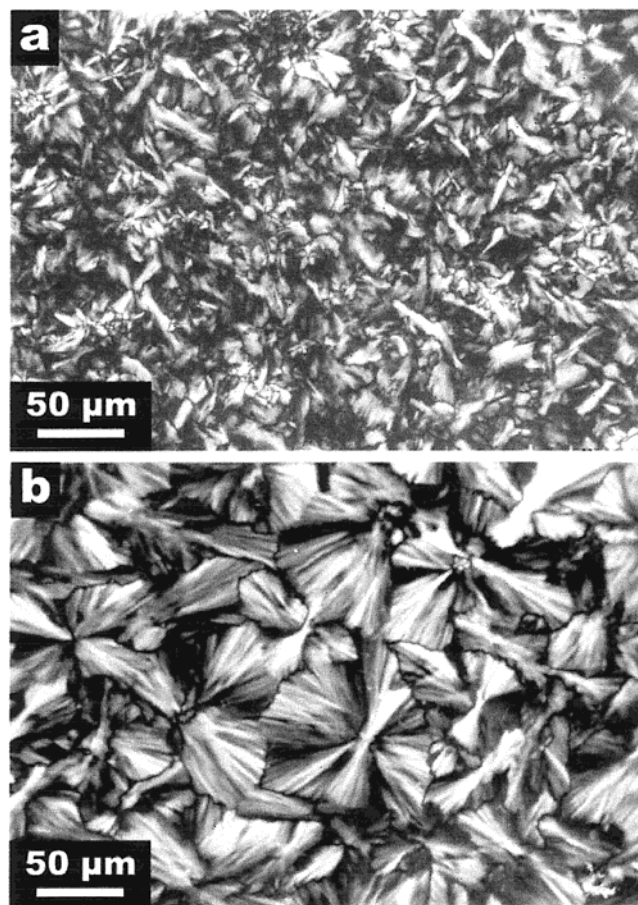


Figure 45. Optical micrographs, between crossed polarizers, of alkane $C_{162}H_{326}$ to which 10 wt % was added of (a) $C_{122}H_{246}$, and (b) $C_{246}H_{494}$. $T_c = 120$ °C. The mixture with the longer-chain guest molecules (b) shows a texture resembling that of polymer spherulites (from ref 204 by permission of American Chemical Society).

indeed formed in the folded-chain crystallization region, but not in the extended-chain region. This would lend support to the cilia hypothesis, in view of the NIF structure. Subsequent work has shown, however, that even extended-chain lamellae splay and diverge, and the angle of divergence increases with increasing degree of supercooling. The idea of transient ciliation has therefore been suggested; the initial crystalline stem length would thus depend on supercooling even within the extended-chain growth regime, the cilium length increasing with increasing supercooling. It must be recognized, however, that the transient cilia would have to be confined to a narrow growth front of the lamellae, since otherwise, without chain-folding, the overcrowding effect would prevent further growth (see Sections II.C and II.J).

Supporting evidence for cilia being responsible for lamellar divergence and the consequent tendency for spherulite formation comes from the morphology of alkane mixtures.²⁰⁴ In Figure 45, optical textures are shown of two mixtures with $C_{162}H_{326}$ the majority component. The sample in Figure 45a has 10 wt % $C_{122}H_{246}$ added, while the sample in Figure 45b has the same amount of added $C_{246}H_{494}$. The morphology in Figure 45b has recognizable features of polymer spherulites, while that in Figure 45a has not. This

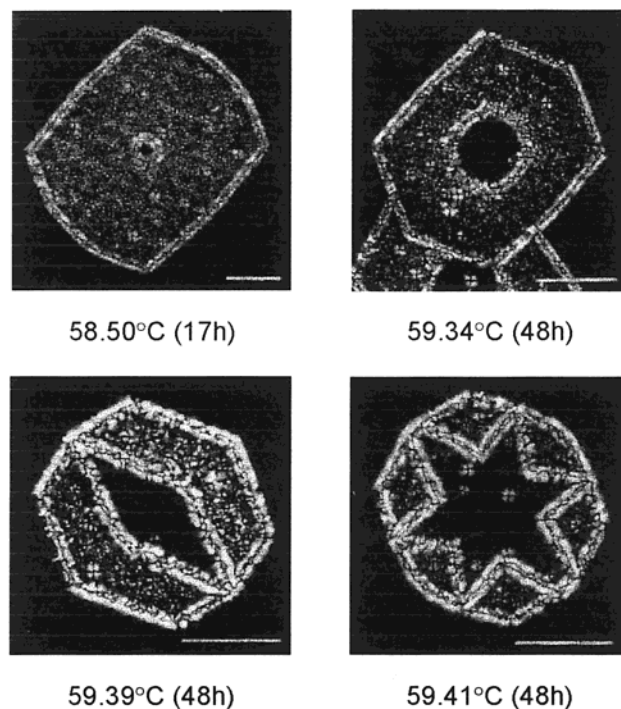


Figure 46. Crystals of PEO fraction $M_n = 6000$ grown from the melt at temperatures indicated, and then quenched to achieve surface decoration by small spherulites. The black undecorated areas are extended chain (from ref 28 by permission of John Wiley & Sons).

is attributed to permanent cilia existing in the semicrystalline form (SCF) of the $C_{162}H_{326}$ - $C_{246}H_{494}$ blend.

D. Lamellar Thickening

Since the thin lamellar crystals of polymers are metastable and owe their shape to criteria of kinetics rather than equilibrium thermodynamics, at elevated temperatures aided by increased mobility, they often thicken. The thickening is normally continuous and logarithmic in time.²¹⁸ However, already the earliest SAXS studies of PEO fractions have shown lamellar thickness to increase in a stepwise manner.²¹⁹ Each step corresponded to one integer folded (IF) form. The quantized nature of lamellar thickening has proven highly advantageous in visualizing the thickening process using different microscopy techniques. Below are three examples illustrating the use of optical, electron, and atomic force microscopy.

Figure 46 shows four crystals of PEO fraction $M_n = 9000$ grown from the melt at the temperatures indicated.²⁸ As in Figure 39, the crystals were “self-decorated” by quenching. Crystallization temperature of 58.50 °C is in the region of once-folded-chain growth, but the other three temperatures are in the transition region between folded and extended chain growth. The folded-chain crystals were grown from a small extended-chain seed. As the octagonal and hexagonal folded-chain crystals in the top row of Figure 46 were growing, the central extended-chain portion was spreading radially at a slower rate, maintaining a circular envelope. Here thickening also involves incorporation of new molecules from the

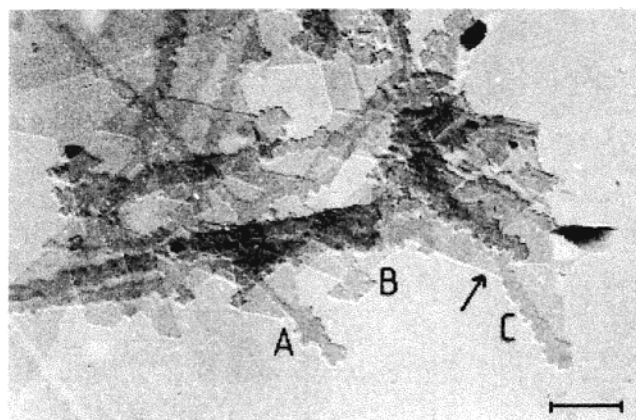


Figure 47. Lozenge-shaped crystals of once-folded alkane $C_{198}H_{398}$ grown from a 0.02% solution in toluene and partially thickened isothermally during annealing at $T_c = 73\text{ }^\circ\text{C}$ for $t = 5\text{ h}$. Marker = 1 micron (from ref 220b by permission of John Wiley & Sons).

surrounding melt. At $T_c = 59.39\text{ }^\circ\text{C}$, the black extended-chain portion is rhombus-shaped and directed along the a -axis. At this temperature, the folded-chain growth in the $[100]$ direction is already slower than the extended-chain growth, hence an extended-chain tip progresses ahead of the folded-chain layer. At $59.41\text{ }^\circ\text{C}$, the folded-chain rate in the $[140]$ direction also drops below the extended-chain rate, hence the four additional arms to the extended-chain star in the pathological crystal in Figure 46d.

Thickening of once-folded and twice-folded n -alkane crystals in solution has been studied by DSC and transmission electron microscopy.^{220,221} Figure 47 shows a group of initially lozenge-shaped once-folded-chain crystals of $C_{198}H_{398}$ (cf. Figure 41a) partially thickened isothermally at T_c while freely suspended in solution.^{220b} Thickening was found to invariably start at an apex followed by rapid spreading of a strip along the sector boundary, i.e., either along the $[100]$ or the $[010]$ direction. At the end of the process a network of crosshatched extended-chain strips is all that remains. Figure 47 contains a number of details illustrative of the progress of thickening. The extended-chain strip, which traverses the crystal, widens with time, consuming the adjacent folded-chain layer (see, e.g., areas marked A and B). It has been proposed that material is transported to the thickened strip by slippage along the $\{110\}$ lattice planes. Such slippage leaves behind smooth $\{110\}$ lamellar edges, as in crystal A. Surface decoration has indeed shown that the fold regularity becomes severely disrupted in those areas that had undergone slippage.

The slippage within a crystal can be seriously impeded either by multilayer crystals or where a portion of the unthickened crystal is bounded on two or more sides by thickened strips. An example of how an overlaying layer inhibits slippage is provided by the crystal marked C in Figure 47. Here it is the left-hand side which had mainly been consumed in the widening of the extended-chain strip. It seems that the slippage of the right-hand side of the crystal had been prevented by the complex overgrowth on that side. In fact, the slippage of the left-hand half had

also ceased when the (110) slip plane reached the overlying second layer nearby. Thus, the portion of the folded-chain layer marked with an arrow could not easily be pulled in by thickening.

Isothermal thickening from F4 to F3 and F3 to F2-folded forms of $C_{294}H_{590}$ crystals in toluene solution shows a rather different pattern.²²¹ Transformation from chains folded in three to chains folded in two ($F3 \rightarrow F2$) destroys any recognizable crystal shape and results in an irregular crystal habit with narrow (20–30 nm) strips of thickened material. Transport of mass required for solid-state thickening is clearly more impeded than in the case of $F2 \rightarrow E$ transformation in $C_{198}H_{398}$. The $F4 \rightarrow F3$ conversion in $C_{294}H_{590}$ crystals did not proceed at all by solid state diffusion, judging by the resulting “picture-frame” F3 crystals. This latter morphology implies that “thickening” occurs through dissolution of the F4 crystal interior and simultaneous F3 precipitation at crystal edges. It should be noted that in polyethylene, thickening does not normally take place at T_c in solution crystallization; if temperature is raised subsequently to about $T_c + 10\text{ }^\circ\text{C}$, picture-frame crystals may appear.²²²

If single layer polymer crystals are deposited on a substrate and annealed, thickening is accompanied by the creation of holes, as pulling in of material from the side to feed the thickened regions is severely restricted.²²³ However, holes can develop on annealing even in multilayer crystals.²²³ Such “Swiss cheese” morphology has also been observed using AFM of annealed once-folded solution-grown crystals of $C_{162}H_{326}$ deposited on mica.²²⁴ The thickening process could in this case also be studied in real time. Figure 48 shows two out of a series of AFM height-contrast images taken at different annealing times. A thickened extended-chain strip is seen to develop and propagate along the edge of the crystal.

Thickening is facilitated considerably when crystal lamellae are stacked on top of one another, reducing the need for large scale transport of matter. Figure 49 shows the changing SAXS curve during continuous heating of a mat of stacked solution-grown crystals of alkane $n\text{-}C_{390}H_{782}$ with the chains initially folded in five (F5).²²⁵ The first and second-order SAXS peaks are seen to move to lower angles in a stepwise fashion, the crystals passing through integer forms $F5 \rightarrow F4 \rightarrow F3 \rightarrow F2$.

E. Implications for Polymer Crystallization Theory

To discuss the implications of the observed crystal growth behavior of model chains, certain issues in polymer crystallization theory need summarizing. The secondary nucleation theory has been the dominant theory for several decades and has undergone numerous modifications since its original establishment by Frank and Tosi²²⁶ and Lauritzen and Hoffman (LH).²²⁷ As mentioned in Section III.A, it assumes that the lateral growth of a crystal lamella of thickness l proceeds by deposition of layer upon layer of stems (straight chain segments) of length l , each layer being nucleated by the deposition of the first stem (see Figure 33). Deposition of the first stem

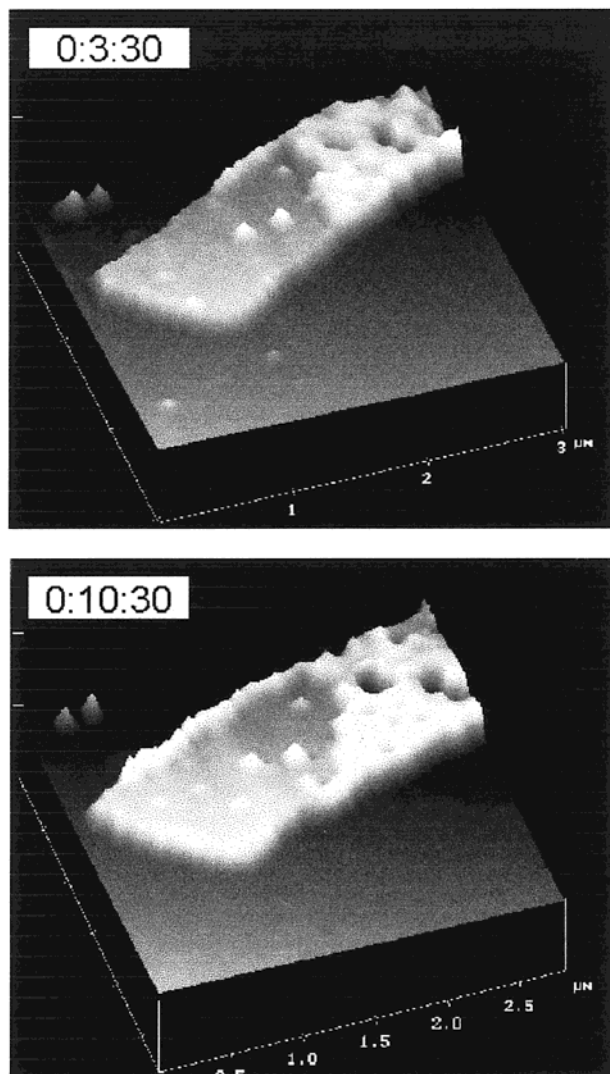


Figure 48. Two out of a sequence of height AFM images of a crystal of $n\text{-C}_{162}\text{H}_{326}$, initially once-folded, recorded during annealing at 100 °C. The extended-chain form propagates along the edge of the crystal (from ref 224 by permission of Elsevier Science).

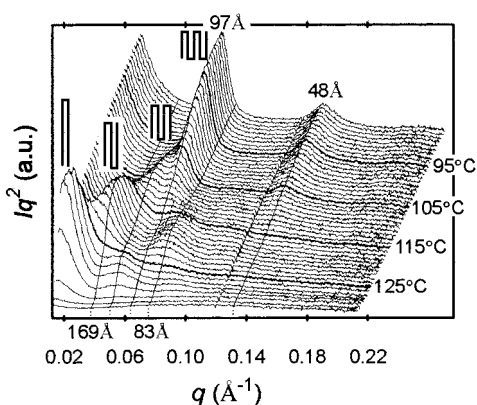


Figure 49. Series of SAXS intensity functions recorded during heating of solution-crystallized $n\text{-C}_{390}\text{H}_{782}$ at 2 deg C/min. The integer forms that the crystals pass through are marked by the corresponding symbols of their molecular conformation (from ref 225).

raises the net free energy by $2bl\sigma - \psi abl\Delta\phi$, where σ is the side-surface free energy, $\Delta\phi$ the bulk free energy of crystallization per unit volume, and ψ is

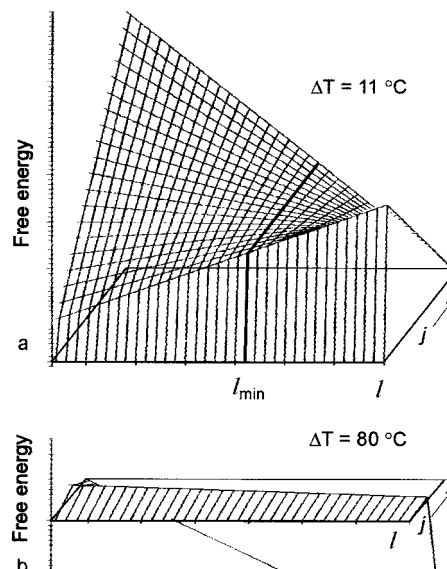


Figure 50. Free energy of a new layer of stems on the lateral growth face of a polymer crystal as a function of stem length l and the number of stems in the layer, j . Calculated according to the Lauritzen-Hoffman theory, with $\psi = 1$. (a) $\Delta T = 11$ °C, (b) $\Delta T = 80$ °C. Standard data for polyethylene were used. Case a predicts $l = l_{\min} + \delta l$ with a small δl , while (b) predicts $l \rightarrow \infty$.

the “apportioning factor” determining what fraction of the crystallization energy had been released at the peak of the barrier during the attachment of a stem.¹⁸³ Deposition of subsequent stems (“substrate completion”) is then fast, since the barrier for each new stem is only $2ab\sigma_e - \psi abl\Delta\phi$ (σ_e is the end-surface energy). According to this surface-energy-based theory, the barrier for deposition of the first stem is highest of all due to the large surface area bl . Provided l is larger than the minimum thickness l_{\min} of crystals stable at a given T_c , attachment of each subsequent stem reduces the free energy of the new layer. This is illustrated in Figure 50a, where the free energy is shown as a function of l and j , j being the number of stems in the layer. For simplicity, Figure 50 shows the situation for $\psi = 1$; for $0 < \psi < 1$, there would be an additional maximum between each j and $j+1$.

The elementary steps in the LH theory are the deposition of the first stem (rate constant A_0), deposition of subsequent stems (A), and removal of a stem (B). The individual rate constants are of the form $\beta \exp[-(\text{barrier})/kT]$, where β contains the viscosity factor etc. Hence,

$$A_0 = \beta \exp[-(2bl\sigma - \psi abl\Delta\phi)/kT] \quad (7a)$$

$$A = \beta \exp[-(2ab\sigma_e - \psi abl\Delta\phi)/kT] \quad (7b)$$

$$B = \beta \exp[-(1 - \psi)abl\Delta\phi/kT] \quad (7c)$$

The whole process is treated as a series of consecutive reactions and the steady-state solution gives the net flux S_l for a given crystal thickness l as

$$S_l = N_0 A_0 \left(1 - \frac{B}{A}\right) \quad (8)$$

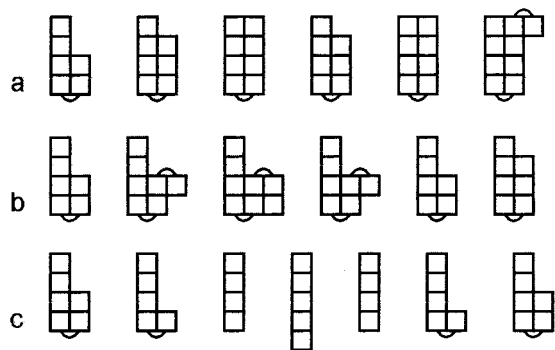


Figure 51. A series of fluctuations at the crystal growth face. The squares represent crystallized chain segments. (a) Steps allowed in the Frank-Tosi model,²²⁶ (b and c) some other possible steps (after ref 4).

N_0 is the total number of stems. Substituting eq 7 into eq 8, we get

$$S_l = \beta N_0 \{ \exp[(-2bl\sigma + \psi abl\Delta\phi)/kT] \{ 1 - \exp[(-abl\Delta\phi + 2ab\sigma_e)/kT] \} \} \quad (9)$$

The second factor in eq 9 (“driving force factor”) increases with increasing l , and for $l > l_{\min} = 2\sigma_e/(\Delta\phi)$, it is positive. At small and moderate ΔT , the first factor (“barrier factor”) decreases with increasing l . Hence $S(l)$ has a maximum. The l -value of the maximum, as well as the average value of l , is somewhat larger than l_{\min} . Thus,

$$\langle l \rangle = l_{\min} + \delta l \quad (9)$$

The secondary nucleation theory is “coarse grain” and makes a serious simplification by treating the stem deposition as a single event. The most conspicuous consequence of this in the application to polymers is the erroneous prediction of δl increasing and diverging at large ΔT , the so-called δl catastrophe.¹⁸³ The increase in l would happen because the large increase in crystallization free energy $\Delta\phi \approx \Delta T\Delta s_f$ (s_f = entropy of fusion) would cause the energy barrier to decrease rather than increase with l , as illustrated in Figure 50b. Setting $\psi < 1$ would reduce but not eliminate the problem; it would in fact only shift the δl upturn to lower temperatures.

Frank and Tosi²²⁶ considered the sequential deposition of stem segments, allowing forward and backward fluctuations, but did not allow folding back until the stem reached l_{\min} , see Figure 51a. Thus, their approach does not eliminate the δl catastrophe. However, Point²²⁸ did consider the multitude of pathways in the deposition of the first (nucleus) stem of a new layer. The stem was allowed to fold after each deposited segment (see Figure 51, panels b and c). The elementary steps in the deposition of the stem were addition and removal of segments, with rate constants A and B , and the net forward rate of folding, C_f . The solution of the steady-state equation gave then the value of $\langle l \rangle$, which was somewhat larger than l_{\min} . This removed the δl catastrophe as it changed the nature of the free energy barrier from energetic to probabilistic (entropic). Forming a long extended stem in a flexible polymer will always be

less probable and thus slower than forming a shorter stem, irrespective of ΔT . Point did not, however, extend this treatment to the deposition of subsequent stems, i.e., layer completion was handled as attachment of complete stems.

The most radical departure from LH theory was that by Sadler,^{185,186,199} whose theory was intended to describe crystallization at higher temperatures, where lateral crystal faces are above their roughening transition temperature T_R . High equilibrium roughness removes the necessity of surface nucleation as there is no surplus free energy associated with a step. The model is fine grain, and each stem is made up of individual segments. In a simple cubic crystal, the roughening transition on a $\{100\}$ surface should occur at $kT\epsilon \approx 0.6$,⁴ where ϵ is the pairwise nearest neighbor attraction energy. If whole stems are treated as nondivisible units on a polymer crystal surface, then ϵ is so large that the surface at equilibrium is always smooth and flat. However, a simple estimate shows that, if polyethylene stems were broken down into segments of no more than six CH_2 units, the surface would be thermodynamically rough. This crude estimate does not take account of connectivity between segments, and there are numerous problems in estimating T_R of such complex systems as polymer crystals. However, Sadler argued that the fact that the $\{100\}$ faces in polyethylene become curved at high temperatures indicates the roughening transition. In contrast, $\{110\}$ faces with somewhat denser packing of surface chains and hence a higher ϵ would have a higher T_R , hence the $\{110\}$ faces remain faceted.

To solve the problem analytically, Sadler studied a simplified model containing a row of stems, i.e., a cut through the crystal normal to the side surface. Monte Carlo simulation was also done in parallel. Surface configurations were allowed to evolve naturally and beyond those in Figure 51b and c. On average there were multiple temporary attachments of stems with $l < l_{\min}$, the outermost stems having the smallest l . The theory could explain most observations in polymer crystallization, such as the temperature dependencies of crystal growth rate and lamellar thickness. The model, like that of Point, avoids the δl catastrophe. Sadler’s model is often referred to as the “roughness-pinning” model. Roughness refers to equilibrium and kinetic surface roughness, resulting from splitting stems into segments and negating the need for nucleation. “Pinning” refers to the adopted rule that a “buried” segment cannot move unless the stems that cover it detach. Thus, a stem is immobilized, or pinned down, even if covered by only temporary unstable attachments with $l < l_{\min}$. The free energy barrier for crystal growth is thus entropic rather than enthalpic, but in contrast to the model by Point, a significant contribution comes from “pinning”.²²⁹

Most experimental observations on polymer crystallization can be interpreted reasonably well by a number of crystallization theories, some of which differ fundamentally in their starting premises. Apart from the δl catastrophe, the experimental ΔT dependencies of crystal thickness and growth rate can

be explained by most theories. Thus, e.g., the free energy barrier is roughly linear in l in both LH theory ($=2lbo$), as well as in the fine-grain theories of Point and Sadler ($-sT = kT \ln(w)^{-1}$, where $w \cong p^n$, p being the number of conformers per segments and n the number of segments in a stem; hence $-sT \propto n \propto l$).

Experimental results on monodisperse model polymers therefore provide much needed further tests for the theories. The self-poisoning minimum in particular can be regarded as one of the key probes, alongside the δl catastrophe and the curved crystal faces. As it happens, in the course of their rate equation analysis Sadler and Gilmer included in their investigation a model with certain energetically preferred stem lengths and indeed observed minima in growth rate vs ΔT .¹⁹⁹ Since no such effect had been observed at the time, the work remained unpublished until the experimental results on alkane $C_{246}H_{494}$ became available.¹⁸⁹ The subsequent theoretical and simulation analysis of the ΔT ²⁰⁰ and concentration¹⁹² dependencies of alkane growth rate was based on Sadler's model. In our opinion, only fine grain theories can describe the minimum. An attempt to interpret it in terms of the coarse-grain LH theory²³⁰ had to resort to highly unusual Arrhenius-type terms and could be disputed on other grounds.²¹⁰ The chances are that Point's model might also predict the minimum if applied to monodisperse chains; up to now, this has not been tested. However, it is almost certain that neither the roughness-pinning theory nor Point's model would predict crystal shapes correctly, the former because it fails to distinguish between nucleation and growth. On the other hand, Point's original fine-grain treatment would not be able to explain the minimum in v , such as that in Figure 42, because it only applies to nucleation and not to growth of new layers.

As mentioned in Section III.C, the fact that the temperature dependence of crystal habits in polyethylene is an almost exact reversal of that in alkanes approaching the rate minimum is an indication that self-poisoning is present in crystallization of the polymer and that it is more pronounced at higher temperatures. Figure 43 tentatively describes the row of stems normal to a self-poisoned surface in a polymer crystal. The situation is the same as that envisaged by Sadler. However, Figure 43 could equally apply to a layer of stems parallel to the surface, in which case it would describe retardation in v , a case not considered by Sadler. Paradoxically, it is the exact shape of rounded crystals of alkanes and polyethylene that point indirectly to poisoning of polymer crystal faces and the similarity with Sadler's model. However, we now know that this model was conceived by mistakenly associating the rounding with nonnucleated growth. At this juncture, it would appear that a synthesis of Sadler's model and the nucleation theory could come close to explaining most experimental observations in polymers as well as in monodisperse model compounds. A similar outcome may potentially be expected from Point's theory, extended to include fine-grain treatment of layer completion.

Several significant developments in polymer crystallization theory have been made more recently, e.g., the two-dimensional nucleation and sliding diffusion theory of Hikosaka,²³¹ the two-stage crystallization model by Strobl,²³² and a number of simulation studies have been carried out and are in progress. Past and future experiments on model compounds will undoubtedly benefit these developments.

IV. Conclusions

Research on model compounds and sharp oligomer fractions has already had a profound effect on our understanding of polymer crystallization and morphology. The availability of monodisperse polymers removes the dependence of this field of science on essentially impure multicomponent experimental systems. It also helps close the gap between polymer science and mainstream chemistry and physics.

The list of achievements made possible with the aid of model compounds includes (1) discovery of integer folding, stepwise lamellar thickening, crystal growth rate transitions, separation of the effects of temperature and crystal thickness in crystallization kinetics; (2) visualization and elucidation of the topology of lamellar thickening, taking advantage of the enhanced quantized thickness contrast; (3) observation and structural characterization of transient noninteger folding and of the subsequent transformations, new insights into primary chain deposition, ciliation, and subsequent rearrangements, of relevance to secondary crystallization in polymers; (4) new 1-D superlattices in mixed long chains, unexpected stability of semicrystalline structures, and experimental determination of the extent of overcrowding at the crystal-amorphous surface; (5) the role of cilia in pure and binary systems, the effect on lamellar branching and spherulite growth; (6) the discovery of self-poisoning and its unusual consequences for crystallization kinetics, the resolution of the effect on the deposition of the first and subsequent stems, discovery of poisoning by shorter chains, the likely effect of self-poisoning on crystallization and morphology of polymers; (7) elucidation of the nature of the fold surface and end surface, determination of the spectral bands due to folds (IR, Raman, NMR), and new insights into chain tilt and surface disorder; (8) improved understanding of the effect of chain length and lamellar thickness on melting point and Raman LAM frequency, derivation of improved values for equilibrium melting point and Young's modulus of polymer chains; (9) better understanding of end-group effects and bilayer formation; and (10) of the effect of specific chemical defects and short and long branches on the crystallization process and the resulting structure.

There is ample scope for future research. For example, new monodisperse oligomers are currently being contemplated, notably aromatic and model biopolymers. Deuterium-labeled long alkanes are being studied by neutron scattering and NMR. Fold surfaces of IF crystals, devoid of amorphous overlayer, may be amenable to studies by different

surface techniques. Primary nucleation and high-pressure studies are underway.

V. List of Symbols and Abbreviations

AFM	atomic force microscopy
b	width of a molecular chain
E	extended chain
E	Young's modulus
F2, F3, ..., $F(m+1)$	chains folded in two, three etc.
Δf	bulk free energy of crystallization
G	crystal growth rate
IF	integer folded
i	rate of initiation (secondary nucleation) of a new row of stems on crystal growth face
j	order of the longitudinal acoustic mode (LAM); number of stems in a layer
L	chain length
l	long period (l_{SAXS} or l_{LAM})
l_c	thickness of the crystalline layer
l_a	thickness of the amorphous or disordered layer
l_s	length of straight chain segment traversing the crystal (stem length)
LAM	longitudinal acoustic mode
m	number of folds per molecular chain
M_n	number average molecular mass
M_n^a	number average molecular mass of an arm in a branched oligomer
n	number of monomer repeat units per chain (e.g. number of carbons in an alkane)
NIF	noninteger folded
ν	Raman frequency
p	number of monomer units in the alternative block in a diblock or tri-block chain
PEO	poly(ethylene oxide)
PET	poly(ethylene terephthalate)
ψ	free energy barrier apportioning parameter
q	modulus of the wavevector, $q = 4\pi(\sin\theta)/\lambda$, where θ is half the scattering angle and λ is radiation wavelength
SAXS	small-angle X-ray scattering
SCF	semicrystalline form
σ	side-surface free energy
σ_e	end- or fold-surface free energy
T_c	crystallization temperature
T_c^m	growth transition temperature between $m-1$ and m folds per molecule
T_m	melting temperature
T_R	roughening transition temperature
$\Delta T = T_m - T_c$	supercooling
TEM	transmission electron microscopy
v	rate of step propagation on a crystal growth face

VI. Acknowledgments

This work was supported by Engineering and Physical Research Council and the Petroleum Research Fund, administered by the American Chemical Society. GU also acknowledges a grant from VBL, University of Hiroshima, during his sabbatical leave.

VII. References

- (1) Wunderlich, B. *Macromolecular physics, Vol. 1: Crystal structure, morphology, defects*; Academic Press: New York, 1973.
- (2) Wunderlich, B. *Macromolecular physics, Vol. 2: Crystal nucleation, growth, annealing*; Academic Press: New York, 1976.
- (3) Keller, A. In *Sir Charles Frank: An Eightieth Birthday Tribute*; Chambers, R. G.; Enderby, J. E.; Keller, A.; Lang, A. R.; Steeds, J. W., Eds.; Adam Hilger: Bristol, 1991.
- (4) Gedde, U. W. *Polymer Physics*; Chapman and Hall, 1995.
- (5) For a review of polymer crystallization theory, see Armitstead, K.; Golbeck-Wood, G. *Adv. Polym. Sci.* **1992**, *100*, 219.
- (6) Jonas, A.; Legras, R.; Scherrenberg, R.; Reynaers, H. *Macromolecules* **1993**, *26*, 526; Dupont, O.; Jonas, A. M.; Nysten, B.; Legras, R.; Adriaensens, P.; Gelan, J. *Macromolecules* **2000**, *33*, 562.
- (7) Rueda, D. R.; Zolotukhin, M. G.; Nequiqueo, G.; Garcia, C.; De La Campa, J. G.; De Abajo, J. *Macromol. Chem. Phys.* **2000**, *201*, 427.
- (8) Keller, A. Lecture presented at Symposium "La Vie", Société de la Vie, Palais de Versailles, June 1977.
- (9) Smith, A. E. *J. Chem. Phys.* **1953**, *21*, 2229.
- (10) Shearer, H. M. M.; Vand, V. *Acta Crystallogr.* **1956**, *9*, 379.
- (11) Pieszek, W.; Strobl, G. R.; Makahn, K. *Acta Crystallogr., Sect. B* **1974**, *30*, 1278.
- (12) Dawson, I. M. *Proc. R. Soc. (London)* **1952**, *A214*, 72.
- (13) Flory, P. J.; Vrij, A. *J. Am. Chem. Soc.* **1963**, *85*, 3548.
- (14) Wunderlich, B.; Czornyj, G. *Macromolecules* **1977**, *10*, 906.
- (15) Yamanobe, T.; Sorita, T.; Komoto, T.; Ando, I.; Sato, H. *J. Mol. Struct.* **1985**, *131*, 267.
- (16) Zerbi, G.; Magni, R.; Gussoni, M.; Moritz, K. H.; Bigotto, A.; Dirlikov, S. *J. Chem. Phys.* **1981**, *75*, 3175.
- (17) Maroncelli, M.; Qi, S. P.; Strauss, H. L.; Snyder, R. G. *J. Am. Chem. Soc.* **1982**, *104*, 6237.
- (18) Ungar, G.; Keller, A. *Colloid Polym. Sci.* **1979**, *257*, 90.
- (19) Zerbi, G.; Piazza, R.; Holland-Moritz, K. *Polymer* **1982**, *23*, 1921.
- (20) Broadhurst, M. G. *J. Res. Natl. Bur. Stand., Sect. A* **1962**, *66*, 241.
- (21) Bassett, D. C.; Block, S.; Piermarini, G. *J. Appl. Phys.* **1974**, *45*, 4146.
- (22) Ungar, G. *Macromolecules* **1986**, *19*, 1317.
- (23) Sirota, E. B.; King, H. E., Jr.; Singer, D. M.; Shao, H. H. *J. Chem. Phys.* **1993**, *98*, 5809.
- (24) Zahn, H.; Pieper, W. *Angew. Chem.* **1961**, *73*, 246.
- (25) Balta-Calleja, F. J.; Keller, A. *J. Polym. Sci. A2* **1963**, *2*, 2151.
- (26) Kern, W.; Davidovits, J.; Rautekus, K. J.; Schmidt, G. F. *Makromol. Chem.* **1961**, *43*, 106.
- (27) Balta-Calleja, F. J.; Keller, A. *J. Polym. Sci. A* **1964**, *2*, 2171.
- (28) Arlie, J. P.; Spegt, P.; Skoulios, A. *C. R. Acad. Sci. Paris* **1965**, *260*, 5774.
- (29) Kovacs, A. J.; Gonthier, A.; Straupe, C. *J. Polym. Sci., Polym. Symp.* **1975**, *50*, 283.
- (30) Buckley, C. P.; Kovacs, A. J. In *Structure of Crystalline Polymers*; Hall, I. H., Ed.; Elsevier-Applied Science: London, 1984; pp 261–307.
- (31) Bidd, I.; Whiting, M. C. *J. Chem. Soc., Chem. Commun.* **1985**, 543; Bidd, I.; Holdup, D. W.; Whiting, M. C. *J. Chem. Soc., Perkin Trans. 1* **1987**, 2455.
- (32) Lee, K. S.; Wegner, G. *Makromol. Chem.-Rapid Commun.* **1985**, *6*, 203.
- (33) Brooke, G. M.; Burnett, S.; Mohammed, S.; Proctor, D.; Whiting, M. C.; *J. Chem. Soc., Perkin Trans. 1* **1996**, 1635.
- (34) Ungar, G.; Stejny, J.; Keller, A.; Bidd, I.; Whiting, M. C. *Science* **1985**, *229*, 386.
- (35) Cheng, S. Z. D.; Chen, J. H.; Zhang, A. Q.; Heberer, D. P. *J. Polym. Sci., Part B: Polym. Phys.* **1991**, *29*, 299.
- (36) Mizushima, S.-I.; Shimanouchi, T. *J. Am. Chem. Soc.* **1949**, *71*, 1320.
- (37) Palmö, K.; Krimm, S. *J. Polym. Sci., Polym. Phys. Ed.* **1996**, *34*, 37.
- (38) Hartley, A.; Leung, Y. K.; Booth, C.; Shepherd, I. W. *Polymer* **1976**, *17*, 355.
- (39) Kim, I.; Krimm, S. *Macromolecules* **1996**, *29*, 7186.
- (40) Strobl, G. R.; Eckel, R. *J. Polym. Sci., Polym. Phys. Ed.* **1976**, *14*, 913.
- (41) Ungar, G. In *Integration of Fundamental Polymer Science and Technology, Vol. 2*; Lemstra, P. J.; Kleintjens, L. A., Ed.; Elsevier Applied Sci.: London, 1988; pp 342–362.
- (42) Snyder, R. G.; Strauss, H. L.; Alamo, R.; Mandelkern, L. *J. Chem. Phys.* **1994**, *100*, 5422.
- (43) Zeng, X. B.; Ungar, G. Unpublished material.
- (44) Khoury, F.; Fanconi, B.; Barnes, J. D.; Bolz, L. H. *J. Chem. Phys.* **1973**, *59*, 5849.
- (45) Minoni, G.; Zerbi, G. *J. Phys. Chem.* **1982**, *86*, 4791.
- (46) Song, K.; Krimm, S. *Macromolecules* **1990**, *23*, 1946.
- (47) Viras, K.; Teo, H. H.; Marshall, A.; Domszy, R. C.; King, T. A.; Booth, C. *J. Polym. Sci., Polym. Phys. Ed.* **1983**, *21*, 919.
- (48) Campbell, C.; Viras, K.; Masters, A. J.; Craven, J. R.; Hao, Z.; Yeates, S. G.; Booth, C. *J. Phys. Chem.* **1991**, *95*, 4647.
- (49) Garner, W. E.; Van Bibber, K.; King, A. M. *J. Chem. Soc.* **1931**, 1533.
- (50) Buckley, C. P.; Kovacs, A. J. *Prog. Colloid Polym. Sci.* **1975**, *58*, 44.
- (51) Nakasone, K.; Urabe, Y.; Takamizawa, K. *Thermochim. Acta* **1996**, *286*, 161.

- (51) Mandelkern, L.; Prasad, A.; Alamo, R. G. *Macromolecules* **1990**, *23*, 3696.
- (52) Carlier, V.; Devaux, J.; Legras, R.; Blundell, D. J. *J. Polym. Sci., Polym. Phys.* **1998**, *36*, 2563.
- (53) Buckley, C. P.; Kovacs, A. J. *Colloid Polym. Sci.* **1976**, *254*, 695.
- (54) Hoffman, J. D. *Polym. Commun.* **1986**, *27*, 39.
- (55) Hoffman, J. D.; Miller, R. L. *Polymer* **1997**, *38*, 3151.
- (56) Ungar, G.; Keller, A. *Polymer* **1986**, *27*, 1835.
- (57) Song, K.; Krimm, S. *Macromolecules* **1989**, *22*, 1504.
- (58) Cheng, S. Z. D.; Zhang, A. Q.; Chen, J. H.; Heberer, D. P. *J. Polym. Sci., Part B: Polym. Phys.* **1991**, *29*, 287.
- (59) Ungar, G.; Zeng, X. B.; Brooke, G. M.; Mohammed, S.; *Macromolecules* **1998**, *31*, 1875.
- (60) Guttman, C. M.; DiMarzio, E. A.; Hoffman, J. D. *Polymer* **1981**, *22*, 1466.
- (61) Zeng, X. B.; Ungar, G.; Spells, S. J. *Polymer* **2000**, *41*, 8775.
- (62) Glatter, O.; Kratky, O. *Small Angle X-ray Scattering*; Academic Press: London, 1982.
- (63) Cheng, S. Z. D.; Chen, J. H.; Zhang, A. Q.; Barley, J. S.; Habenschuss A.; Schack, P. R.; *Polymer* **1992**, *33*, 1140.
- (64) Kovacs, A. J.; Gonthier, A. *Kolloid Z. Z. Polym.* **1972**, *250*, 530.
- (65) Campbell, C.; Viras, K.; Booth, C. *J. Polym. Sci., Part B: Polym. Phys.* **1991**, *29*, 1613.
- (66) Yoon, D. Y.; Flory, P. J. *Faraday Discuss. Chem. Soc.* **1979**, *68*, 288.
- (67) Hoffman, J. D.; Davis, G. T. In *Polymer Surfaces*; Clark, D. T.; Feast, W. J., Ed.; John Wiley & Sons: Chichester 1978; pp 259–268.
- (68) Ungar, G.; Organ, S. J. *Polym. Commun.* **1987**, *28*, 232.
- (69) Wittmann, J. C.; Lotz, B. *J. Polym. Sci., Polym. Phys. Ed.* **1985**, *25*, 205.
- (70) Painter, R. C.; Havens, J.; Hart, W. W.; Koenig, J. L. *J. Polym. Sci., Polym. Phys. Ed.* **1977**, *15*, 1223.
- (71) Spells, S. J.; Organ, S. J.; Keller, A.; Zerbi, G. *Polymer* **1987**, *28*, 697.
- (72) Lee, K.-S.; Wegner, G.; Hsu, S. L. *Polymer* **1987**, *28*, 889.
- (73) Strobl, G. R.; Hagedorn, W. *J. Polym. Sci., Polym. Phys. Ed.* **1978**, *16*, 1181.
- (74) Strobl, G. R. *Kolloid Z. Z. Polym.* **1970**, *250*, 1039.
- (75) Zeng, X. B.; Ungar, G. *Polymer* **1998**, *39*, 4523.
- (76) Ungar, G. In *Characterization of solid polymers*; Spells, S. J., Ed.; Chapman and Hall: London, 1994; pp 56–121.
- (77) Zeng, X. B.; Ungar, G. Unpublished work.
- (78) Brooke, G. M.; Mohammed, S.; Whiting, M. C. *J. Chem. Soc., Perkin Trans. 1* **1997**, *22*, 3371.
- (79) Brooke, G. M.; Mohammed, S.; Whiting, M. C. *Polymer* **1999**, *49*, 773.
- (80) Atkins, E. D. T.; Hill, M. J.; Jones, N. A.; Sikorski, P. *J. Mater. Sci.* **2000**, *35*, 5179.
- (81) Jones, N. A.; Sikorski, P.; Atkins, E. D. T.; Hill, M. J. *Macromolecules* **2000**, *3*, 4146.
- (82) Cooper, S. J.; Atkins, E. D. T.; Hill, M. J. *Macromolecules* **1998**, *31*, 5032.
- (83) Bellinger, M. A.; Waddon, A. J.; Atkins, E. D. T.; MacKnight, W. J. *Macromolecules* **1994**, *27*, 2130.
- (84) Atkins, E. D. T.; Hill, M. J.; Hong, S. K.; Keller, A.; Organ, S. J. *Macromolecules* **1992**, *25*, 917.
- (85) Cooper, S. J.; Atkins, E. D. T.; Hill, M. J. *Macromolecules* **1998**, *31*, 1, 8947.
- (86) (a) McGrath, K. P.; Fournier, M. J.; Mason, T. L.; Tirrell, D. A. *J. Am. Chem. Soc.* **1992**, *114*, 727. (b) Krejchi, M. T.; Atkins, E. D. T.; Waddon, A. J.; Fournier, M. J.; Mason, T. L.; Tirrell, D. A. *Science* **1994**, *265*, 1427.
- (87) Panitch, A.; Matsuki, K.; Cantor, E. J.; Cooper, S. J.; Atkins, E. D. T.; Fournier, M. J.; Mason, T. L.; Tirrell, D. A. *Macromolecules* **1997**, *30*, 42.
- (88) Fraser, R. D. B.; MacRae, T. P.; Stewart, F. H. C.; Suzuki, E. *J. Mol. Biol.* **1965**, *11*, 706.
- (89) Lotz, B.; Keith, H. D. *J. Mol. Biol.* **1971**, *61*, 201.
- (90) Deguchi, Y.; Fournier, M. J.; Mason, T. L.; Tirrell, D. A. *J. Macromol. Sci., Pure Appl. Chem.* **1994**, *A31*, 1691.
- (91) (a) Krejchi, M. T.; Cooper, S. J.; Deguchi, Y.; Atkins, E. D. T.; Fournier, M. J.; Mason, T. L.; Tirrell, D. A. *Macromolecules* **1997**, *30*, 5012. (b) Parkhe, A. D.; Cooper, S. J.; Atkins, E. D. T.; Fournier, M. J.; Mason, T. L.; Tirrell, D. A. *Int. J. Biol. Macromol.* **1998**, *23*, 251.
- (92) Ungar, G. *Am. Chem. Soc. Polym. Prepts.* **1990**, *31* (2), 108.
- (93) Sullivan, P. K.; Weeks, J. J. *J. Res. Natl. Bur. Stand., Sect. A* **1970**, *74*, 203.
- (94) Nukushina, Y.; Itoh, Y.; Fischer, E. W. *J. Polym. Sci., Polym. Lett.* **1965**, *3*, 383.
- (95) Möller, M.; Cantow, H. J.; Drotloff, H.; Emeis, D. *Makromol. Chem.* **1986**, *187*, 1237.
- (96) Keith, H. D.; Padden, F. J. *Macromolecules* **1996**, *29*, 7776.
- (97) Abo el Maaty, M. I.; Bassett, D. C. *Polymer* **2001**, *42*, 4957.
- (98) Hay, I. L.; Keller, A. *J. Mater. Sci.* **1966**, *1*, 41; Hay, I. L.; Keller, A. *J. Mater. Sci.* **1967**, *2*, 538; Hay, I. L.; Keller, A. *J. Mater. Sci.* **1968**, *3*, 646.
- (99) Khoury, F. *Faraday Discuss. Chem. Soc.* **1979**, *68*, 404.
- (100) Bassett, D. C.; Hodge, A. M. *Proc. R. Soc. London A* **1981**, *377*, 25.
- (101) Gautam, S.; Balijepalli, S.; Rutledge, G. C. *Macromolecules* **2000**, *33*, 9136.
- (102) Takamizawa, K.; Ogawa, Y.; Oyama, T. *Polym. J.* **1982**, *14*, 441.
- (103) de Silva, D. S. M.; Gorce, J. P.; Boda, E.; Zeng, X. B.; Ungar, G.; Spells, S. J. Manuscript in preparation.
- (104) Hoffman, J. D.; Weeks, J. J. *J. Chem. Phys.* **1965**, *42*, 4301.
- (105) Brooke, G. M.; Farren, C.; Harden, A.; Whiting, M. C. *Polymer* **2001**, *42*, 2777.
- (106) Zeng, X. B.; Ungar, G. Unpublished material.
- (107) Sadler, D. M. *Faraday Discuss. Chem. Soc.* **1979**, *68*, 106.
- (108) Sikorski, P.; Atkins, E. D. T. *Macromolecules* **2001**, *34*, 4788.
- (109) Kay, H. F.; Newman, B. A. *Acta Crystallogr., Sect. B* **1968**, *B24*, 615.
- (110) Groth, P. *Acta Chem. Scand., Ser. A* **1979**, *A33*, 199.
- (111) Trzebiatowski, T.; Dräger, M.; Strobl, G. R. *Makromol. Chem.* **1982**, *183*, 731.
- (112) Schill, G.; Logemann, E.; Fritz, H. *Chem. Ber.* **1976**, *109*, 497.
- (113) Spells, S. J.; Keller, A.; Sadler, D. M. *Polymer* **1984**, *25*, 749.
- (114) Stocker, W.; Bar, G.; Kunz, M.; Moller, M.; Magonov, S. N.; Cantow, H.-J. *Polym. Bull.* **1991**, *26*, 215.
- (115) Grossmann, H. P.; Arnold, R.; Bürkle, K. R. *Polym. Bull.* **1980**, *3*, 135.
- (116) Petraccone, V.; Corradini, P.; Allegra, L. *J. Polym. Sci., Part C: Polym. Symp.* **1972**, *38*, 419.
- (117) Möller, M.; Gronski, W.; Cantow, H. J.; Höcker, H. *J. Am. Chem. Soc.* **1984**, *106*, 5093.
- (118) Grossmann, H. P. *Polym. Bull.* **1981**, *5*, 137.
- (119) Kögler, G.; Drotloff, H.; Möller, M. *Mol. Cryst. Liq. Cryst.* **1987**, *153*, 179.
- (120) Vaughan, A. S.; Ungar, G.; Bassett, D. C.; Keller, A. *Polymer* **1985**, *26*, 726.
- (121) Yan, Z. G.; Yang, Z.; Price, C.; Booth, C. *Makromol. Chem., Rapid Commun.* **1993**, *14*, 725.
- (122) Cooke, J.; Viras, K.; Yu, G. E.; Sun, T.; Yonemitsu, T.; Ryan, A. J.; Price, C.; Booth, C. *Macromolecules* **1998**, *31*, 3030.
- (123) Chenevert, R.; D'Astous, L. *J. Heterocycl. Chem.* **1986**, *23*, 1785.
- (124) Gibson, H. W., et al. *J. Org. Chem.* **1994**, *59*, 2186.
- (125) Yang, Z.; Yu, G. E.; Cooke, J.; AliAdib, Z.; Viras, K.; Matsuura, H.; Ryan, A. J.; Booth, C. *J. Chem. Soc., Faraday Trans.* **1996**, *92*, 3173.
- (126) Yang, Z.; Cooke, J.; Viras, K.; Gorry, P. A.; Ryan, A. J.; Booth, C. *J. Chem. Soc., Faraday Trans.* **1997**, *93*, 4033.
- (127) Viras, K.; Yan, Z. G.; Price, C.; Booth, C.; Ryan, A. J. *Macromolecules* **1995**, *28*, 104.
- (128) Grossmann, H. P.; Böstler, H. *Polym. Bull.* **1981**, *5*, 175.
- (129) Hasek, J.; Jecny, J.; Langer, V.; Huml, K.; Sedlacek, P. *Acta Crystallogr., Sect. B* **1982**, *38*, 2710.
- (130) Kitano, Y.; Ashida, T. *Polym. J.* **1992**, *24*, 1099.
- (131) Kitano, Y.; Ishitani, A.; Ashida, T. *Polym. J.* **1991**, *23*, 949.
- (132) Clarson, S. J.; Dodgson, K.; Semlyen, J. A. *Polymer* **1985**, *26*, 930.
- (133) Percec, V.; Asandei, A. D.; Chu, P. *Macromolecules* **1996**, *29*, 3736.
- (134) Keller, A.; Udagawa, Y. *J. Polym. Sci., Pt. A-2* **1970**, *8*, 19.
- (135) Barnes, W. J.; Price, F. *Polymer* **1964**, *5*, 283.
- (136) Abrahamson, S.; v. Sydow, E. *Acta Crystallogr.* **1954**, *7*, 591.
- (137) Ungar, G.; Zeng, X. B. *Macromolecules* **1999**, *32*, 3543.
- (138) Zeng, X. B.; Ungar, G. Manuscript to be published.
- (139) Cheng, S. Z. D.; Wu, S. S.; Chen, J. H.; Zhuo, Q. H.; Quirk, R. P.; Von Meerwall, E. D.; Hsiao, B. S.; Habenschuss, A.; Zsack, P. R. *Macromolecules* **1993**, *26*, 5105.
- (140) Hopken, J.; Moller, M. *Macromolecules* **1992**, *25*, 2482.
- (141) Twieg, R.; Rabolt, J.; Russell, T.; Farmer, B. *Abstr. Pap. Am. Chem. Soc.* **1984**, *187*, (Apr.) 17-Poly.
- (142) Yeates, S. G.; Booth, C. *Makromol. Chem.-Macromol. Chem. Phys.* **1985**, *186*, 2663.
- (143) Craven, J. R.; Hao, Z.; Booth, C. *J. Chem. Soc., Faraday Trans.* **1991**, *87*, 1183.
- (144) Campbell, C.; Viras, K.; Richardson, M. J.; Masters, A. J.; Booth, C. *Makromol. Chem., Macromol. Chem. Phys.* **1993**, *194*, 799.
- (145) Hamley, I. W.; Wallwork, M. L.; Smith, D. A.; Fairclough, J. P. A.; Ryan, A. J.; Mai, S. M.; Yang, Y. W.; Booth, C. *Polymer* **1998**, *39*, 3321.
- (146) Lee, S.-W.; Chen, E.-Q.; Zhang, A.; Yoon, Y.; Moon, B.-S.; Lee, S.; Harris, F. W.; Cheng, S. Z. D.; von Meerwall, E. D.; Hsiao, B. S.; Verma, R.; Lando, J. B. *Macromolecules* **1996**, *29*, 8816.
- (147) Chen, E.-Q.; Lee, S.-W.; Zhang, A.; Moon, B.-S.; Honigfort, P. S.; Mann, I.; Lin, H.-M.; Harris, F. W.; Cheng, S. Z. D.; Hsiao, B. S.; Yeh, F. *Polymer* **1999**, *40*, 4543.
- (148) Chen, E.-Q.; Lee, S.-W.; Zhang, A.; Moon, B.-S.; Mann, I.; Harris, F. W.; Cheng, S. Z. D.; Hsiao, B. S.; Yeh, F.; von Meerwall, E. D. In *Scattering from Polymers*, ACS series **2000**, *739*, 118.
- (149) Chen, E.-Q.; Lee, S.-W.; Zhang, A.; Moon, B.-S.; Mann, I.; Harris, F. W.; Cheng, S. Z. D.; Hsiao, B. S.; Yeh, F.; von Meerwall, E. D.; Grubb, D. T. *Macromolecules* **1999**, *32*, 4784.
- (150) Driver, M. A. N.; Klein, P. G. *Macromol. Symp.* **1999**, *141*, 263.
- (151) Zeng, X. B.; Ungar, G. Manuscript in preparation.

- (152) Mazee, W. M. *Anal. Chim. Acta* **1957**, *17*, 97.
- (153) Nechitailo, N. A.; Topchiev, A. V.; Rozenberg, L. M.; Terenteva, E. M. *Russian Journal of Physical Chemistry (English translation)* **1960**, *34* (12), 1268.
- (154) Mnyukh, Yu. V. *J. Struct. Chem. (English translation)* **1960**, *1* (3), 346.
- (155) Kitaigorodskii, A. *Organic Chemical Crystallography*; Consultants Bureau: New York, 1961.
- (156) Matheson, R. R., Jr.; Smith, P. *Polymer* **1985**, *26*, 288.
- (157) Rajabalee, F.; Metivaud, V.; Mondieig, D.; Haget, Y.; Cuevas-Diarte, M. A. *J. Mater. Res.* **1999**, *14*, 2644.
- (158) Luth, H.; Nyburg, S. C.; Robinson, P. M.; Scott, H. G. *Mol. Cryst. Liq. Cryst.* **1974**, *27*, 337.
- (159) Gerson, A. R.; Nyburg, S. C. *Acta Crystallogr., Sect. B* **1994**, *50*, 252.
- (160) Ungar, G.; Masic, N. *J. Phys. Chem.* **1985**, *89*, 1036.
- (161) Doucet, J.; Denicolo, I.; Craievich, A. F.; Collet, A. *J. Chem. Phys.* **1981**, *75*, 5125.
- (162) Denicolo, I.; Craievich, A. F.; Doucet, J. *J. Chem. Phys.* **1984**, *80*, 6200.
- (163) Dorset, D. L. *Macromolecules* **1985**, *18*, 2158; Dorset, D. L. *Macromolecules* **1986**, *19*, 2965; Dorset, D. L. *Macromolecules* **1987**, *20*, 2782; Dorset, D. L. *Macromolecules* **1990**, *23*, 623.
- (164) Kim, Y.; Strauss, H. L.; Snyder, R. G. *J. Phys. Chem.* **1989**, *93*, 3 (1), 485.
- (165) Clavell-Grunbaum, D.; Strauss, H. L.; Snyder, R. G. *J. Phys. Chem. B* **1997**, *101* (3), 335.
- (166) Sirota, E. B.; King, H. E., Jr.; Shao, H. H.; Singer, D. M. *J. Phys. Chem.* **1995**, *99*, 798.
- (167) Basson, I.; Reynhardt, E. C. *J. Chem. Phys.* **1991**, *95* (2), 1215.
- (168) Yamamoto, T.; Nozaki, K. *Polymers* **1994**, *35*, 3340; Yamamoto, T.; Nozaki, K. *Polymers* **1995**, *36*, 2505; Yamamoto, T.; Nozaki, K. *Polymers* **1997**, *38*, 2643.
- (169) Dorset, D. L.; Snyder, R. G. *J. Phys. Chem.* **1996**, *100*, 9848.
- (170) Dorset, D. L. *J. Phys. Chem. B* **1997**, *101*, 4970.
- (171) Gilbert, E. P. *J. Phys. Chem. Chem. Phys.* **1999**, *1*, 5209.
- (172) Chevallier, V.; Provost, E.; Bourdet, J. B.; Bouroukba, M.; Ptitjean, D.; Dirand, M. *Polymer* **1999**, *40*, 2121, 2129.
- (173) Lauritzen, J. I., Jr.; Passaglia, E.; DiMazio, E. A. *J. Res. Natl. Bur. Stand., Sect. A* **1967**, *71* (4), 245.
- (174) Asbach, G. I.; Kilian, H.-G.; Starcke, Fr. *Colloid Polym. Sci.* **1982**, *260*, 151.
- (175) Bonsor, D. H.; Bloor, D. *J. Mater. Sci.* **1977**, *12*, 1559.
- (176) Zeng, X. B.; Ungar, G. *Phys. Rev. Lett.* **2001**, *86*, 4875.
- (177) (a) Zeng, X. B.; Ungar, G. *Macromolecules* **2001**, *34*, 6945. (b) Zeng, X. B.; Ungar, G. *Polymer* **2002** (in press).
- (178) DiMarzio, E. A.; Guttman, C. M. *Polymer* **1980**, *21*, 733.
- (179) Mansfield, M. L. *Macromolecules* **1988**, *21*, 126.
- (180) Balijepalli, S.; Rutledge, G. C. *J. Chem. Phys.* **1998**, *109*, 6523; *Macromol. Symp.* **1998**, *133*, 71.
- (181) Boda, E.; Zeng, X. B.; Ungar, G. Manuscript in preparation.
- (182) Hoffman, J. D. *Macromolecules* **1986**, *19*, 1124.
- (183) Hoffman, J. D.; Davis, G. T.; Lauritzen, J. I., Jr. In *Treatise on Solid State Chemistry*; Hannay, N. B., Ed.; Plenum Press: New York, 1976; Vol. 3, Chapter 7, pp 497–614.
- (184) Hoffman, J. D. *Macromolecules* **1985**, *18*, 772.
- (185) Sadler, D. M. *J. Polym. Sci., Polym. Phys. Ed.* **1985**, *23*, 1533.
- (186) Sadler, D. M. *Polymer* **1983**, *24*, 1401.
- (187) Point, J. J.; Kovacs, A. J. *Macromolecules* **1980**, *13*, 399.
- (188) Toda, A. *J. Phys. Soc. Jpn.* **1986**, *55*, 3419.
- (189) Ungar, G.; Keller, A. *Polymer* **1987**, *28*, 1899.
- (190) Organ, S. J.; Ungar, G.; Keller, A. *Macromolecules* **1989**, *22*, 1995.
- (191) Organ, S. J.; Keller, A.; Hikosaka, M.; Ungar, G. *Polymer* **1996**, *37*, 2517.
- (192) Ungar, G.; Mandal, P.; Higgs, P. G.; de Silva, D. S. M.; Boda, E.; Chen, C. M. *Phys. Rev. Lett.* **2000**, *85*, 4397.
- (193) Boda, E.; Ungar, G.; Brooke, G. M.; Burnett, S.; Mohammed, S.; Proctor, D.; Whiting, M. C. *Macromolecules* **1997**, *30*, 4674.
- (194) Organ, S. J.; Barham, P. J.; Hill, M. J.; Keller, A.; Morgan, R. L. *J. Polym. Sci., Pt. B: Polym. Phys.* **1997**, *35*, 775.
- (195) Sutton, S. J.; Vaughan, A. S.; Bassett, D. C. *Polymer* **1996**, *37*, 5735.
- (196) Hobbs, J. K.; Hill, M. J.; Barham, P. J. *Polymer* **2001**, *42*, 2167.
- (197) Morgan, R. L.; Barham, P. J.; Hill, M. J.; Keller, A.; Organ, S. J. *J. Macromol. Sci., Phys. B* **1998**, *37*, 319.
- (198) Cheng, S. Z. D.; Chen, J. H. *J. Polym. Sci.; Part B: Polym. Phys.* **1991**, *29*, 311.
- (199) Sadler, D. M.; Gilmer, G. H. *Polym. Commun.* **1987**, *28*, 243.
- (200) Higgs, P. G.; Ungar, G. *J. Chem. Phys.* **1994**, *100*, 640.
- (201) Higgs, P. G.; Ungar, G. *J. Chem. Phys.* **2001**, *114*, 6958.
- (202) Fisher, R. A. *Ann. Eugenics* **1937**, *7*, 355.
- (203) de Silva, D. S. M.; Ungar, G.; Zeng, X. B. Manuscript in preparation.
- (204) Hosier, I. L.; Bassett, D. C.; Vaughan, A. S. *Macromolecules* **2000**, *33*, 8781.
- (205) Keith, H. D. *J. Appl. Phys.* **1964**, *35*, 3115.
- (206) Mansfield, M. L. *Polymer* **1988**, *29*, 1755.
- (207) Toda, A. *Polymer* **1991**, *32*, 771.
- (208) Point, J. J.; Villers, D. *J. Cryst. Growth* **1991**, *114*, 228.
- (209) Frank, F. C. *J. Cryst. Growth* **1974**, *22*, 233.
- (210) Ungar, G. In *Polymer Crystallization*; Dosiere, M., Ed.; NATO ASI Series; Kluwer: Dordrecht, 1993; pp 63–72.
- (211) Ungar, G.; Putra, E. G. R. *Macromolecules* **2001**, *34*, 5180.
- (212) Organ, S. J.; Keller, A. *J. Mater. Sci.* **1985**, *20*, 1571.
- (213) Toda, A. *Faraday Discuss.* **1993**, *95*, 129.
- (214) Putra, E. G. R.; Ungar, G. Submitted for publication.
- (215) Hoffman, J. D.; Miller, R. L. *Macromolecules* **1989**, *22*, 3038, 3502; Hoffman, J. D.; Miller, R. L. *Polymer* **1991**, *32*, 963.
- (216) Khoury, F. *J. Appl. Phys.* **1963**, *34*, 73.
- (217) Hosier, I. L.; Bassett, D. C. *Polymer* **2000**, *41*, 8801.
- (218) Fischer, E. W.; Schmidt, G. F. *Angew. Chem.* **1962**, *74*, 551.
- (219) Spegt, P. *Makromol. Chem.* **1970**, *139*, 139.
- (220) (a) Ungar, G.; Organ, S. J. *J. Polym. Sci., Part B: Polym. Phys. Ed.* **1990**, *28*, 2353. (b) Organ, S. J.; Ungar, G.; Keller, A. *J. Polym. Sci., Part B: Polym. Phys. Ed.* **1990**, *28*, 2365.
- (221) Hobbs, J. K.; Hill, M. J.; Barham, P. J. *Polymer* **2000**, *41*, 8761.
- (222) Holland, V. F. *J. Appl. Phys.* **1964**, *35*, 59; Blackadder, D. A.; Schleinitz, H. M. *Polymer* **1986**, *7*, 603.
- (223) Geil, P. H. *Polymer Single Crystals*; Wiley: New York, 1963; Chapter 5.
- (224) Winkel, A. K.; Hobbs, J. K.; Miles, M. J. *Polymer* **2000**, *41*, 8791.
- (225) Boda, E.; Ungar, G.; Zeng, X. B. Manuscript in preparation.
- (226) Frank, F. C.; Tosi, M. *Proc. R. Soc. (London)* **1961**, *A263*, 323.
- (227) Lauritzen, J. I., Jr.; Hoffman, J. D. *J. Res. Natl. Bur. Stand., Sect. A* **1960**, *64*, 73; Hoffman, J. D.; Lauritzen, J. I., Jr. *J. Res. Natl. Bur. Stand., Sect. A* **1961**, *65*, 73.
- (228) Point, J. J. *Macromolecules* **1979**, *12*, 770; Point, J. J. *Discuss. Faraday Soc.* **1979**, *68*, 167.
- (229) Sadler, D. M. *Nature* **1987**, *326*, 174.
- (230) Hoffman, J. D. *Polymer* **1992**, *32*, 2828.
- (231) Hikosaka, M. *Polymer* **1990**, *31*, 458.
- (232) Heck, B.; Hugel, T.; Iijima, M.; Strobl, G. *Polymer* **2000**, *41*, 8839.

CR990130U